Materials Science & Engineering C 131 (2021) 112477

Contents lists available at ScienceDirect

Materials Science & Engineering C

journal homepage: www.elsevier.com/locate/msec

Engineering chitosan nano-cocktail containing iron oxide and ceria: A two-in-one approach for treatment of inflammatory diseases and tracking of material delivery

Yuao Wu [a,b], Gary Cowin [d], Shehzahdi S. Moonshi [a], Huong D.N. Tran [a,b], Najma Annuria Fithri [a], Andrew K. Whittaker [b,e], Run Zhang [b], Hang T. Ta [a,b,c,*]

[a] Queensland Micro- and Nanotechnology Centre, Griffith University, Brisbane 4111, Australia
[b] Australian Institute for Bioengineering and Nanotechnology, University of Queensland, Brisbane 4072, Australia
[c] School of Environment and Science, Griffith University, Brisbane 4111, Australia
[d] Centre of Advanced Imaging, University of Queensland, Brisbane 4072, Australia
[e] ARC Centre of Excellence in Convergent Bio-Nano Science and Technology, The University of Queensland, Brisbane, QLD 4072, Australia

ARTICLE INFO

Keywords:
Anti-inflammatory
Anti-fibrosis
Magnetic resonance imaging
Cerium oxide
Iron oxide

ABSTRACT

In this study, modular two-in-one nano-cocktails were synthesised to provide treatment of inflammatory diseases and also enable tracking of their delivery to the disease sites. Chitosan nano-cocktails loaded with treatment module (cerium oxide nanoparticles) and imaging module (iron oxide nanoparticles) were synthesised by electrostatic self-assembly (Chit-IOCO) and ionic gelation method (Chit-TPP-IOCO), respectively. Their MRI capability, anti-inflammatory and anti-fibrosis ability were investigated. Results demonstrated that Chit-IOCO significantly reduced the expression of TNF-α and COX-2, while Chit-TPP-IOCO reduced IL-6 in the LPS-stimulated macrophages RAW264.7. Cytotoxicity studies showed that the nano-cocktails inhibited the proliferation of macrophages. Additionally, Chit-IOCO exhibited higher in vitro MRI relaxivity than Chit-TPP-IOCO, indicating that Chit-IOCO is a better MRI contrast agent in macrophages. It was possible to track the delivery of Chit-IOCO to the inflamed livers of CCl_4-treated C57BL/6 mice, demonstrated by a shortened T_2* relaxation time of the livers after injecting Chit-IOCO into mice. In vivo anti-inflammatory and blood tests demonstrated that Chit-IOCO reduced inflammation-related proteins (TNF-a, iNOS and Cox-2) and bilirubin in CCl_4 treated C57BL/6. Histology images indicated that the nano-cocktails at the treatment doses did not affect the organs of the mice. Importantly, the nano-cocktail reduced fibrosis of CCl_4-treated mouse liver. This is the first reported data on the anti-inflammation and anti-fibrosis efficacy of Chit-IOCO in C57BL/6 mouse liver inflammation model. Overall, Chit-IOCO nanoparticles have shown great potential in MR imaging/detecting and treating/therapeutic capabilities for inflammatory diseases.

1. Introduction

Hepatopathy refers to a group of hepatic diseases that disrupts normal liver function. Hepatitis particularly has threatened human health since a long time ago. A recent study confirmed that the earliest hepatitis could be traced back to a mummy 4500 years ago [1]. Statistics from the World Health Organization (WHO) revealed that 325 million people worldwide have been infected by chronic hepatitis B virus (HBV) or hepatitis C virus (HCV) by 2017 [2]. Bilirubin and alanine transaminase (ALT) are two important biochemical indicators [3] that are commonly used for biochemical detection of liver dysfunction in the liver inflammatory model [4]. Additionally, several cytokines are overexpressed during the progression of liver inflammation and fibrosis. Briefly, hepatic stellate cells are activated from its quiescent state when liver tissue is inflamed. This triggers the recruitment and activation of leukocytes and Kupffer cells (stellate macrophages) to regulate the behaviour of stellate cells by producing cytokines and other inflammatory mediators to resolve inflammation. These activated macrophages are characterised by increased expression of reactive oxygen species (ROS) and proinflammatory cytokines, including tumor necrosis factor-α (TNF-α), interleukin 6 (IL-6), and inducible NO synthase (iNOS). Subsequently, these pro inflammatory cytokines converts stellate cells to

* Corresponding author at: Queensland Micro- and Nanotechnology Centre, Griffith University, Brisbane 4111, Australia.
E-mail address: h.ta@griffith.edu.au (H.T. Ta).

https://doi.org/10.1016/j.msec.2021.112477
Received 13 May 2021; Received in revised form 19 September 2021; Accepted 1 October 2021
Available online 18 October 2021

myofibroblasts and collagen produced by these myofibroblasts eventually causes liver fibrosis [5,6] (Fig. 1). Besides, cyclooxygenases 2 (COX-2) is involved in the synthesis of prostaglandin E2 (PGE2) and accelerates the progression of inflammation [7]. In addition, IL-6 is a critical pro-proliferation factor in hepatitis to help the regeneration of liver tissue [8].

Cerium oxides displayed anti-ROS ability [9] due to its convertible surface valence whereby both trivalent cerium atoms (Ce^{3+}) and tetravalent cerium atoms (Ce^{4+}) are on the surface of cerium oxide [10]. Cerium oxide nanoparticles can reduce the gene expression of a series of inflammation-related cytokines (TNF-a, Cox-2 and iNOS) in the liver of carbon tetrachloride (CCl_4)-inducted rats [11,12]. Additionally, it was reported that cerium oxide nanoparticles can protect monocrotaline-induced liver damage [13].

Superparamagnetic iron oxide nanoparticles (SPION) are widely used as MRI contrast agents in the diagnosis of various diseases in both preclinical [14–30] and clinical studies [31]. Typically, Resovist® (Bayer Healthcare, SHU-555A, 120 to 180 nm) and Feridex I.V.® (Berlex Laboratories, AMI-25, 60 nm) were two famous commercial iron oxide-based MRI contrast agents that paved the way for liver imaging in clinical practices. Feridex I.V.® was withdrawn from the market due to the lack of clinical users, economic reasons and lower MR imaging efficiency than gadolinium [32,33]. Nonetheless, several studies revealed that the toxicity of gadolinium limits its applications in clinical translation [34]. Therefore, there is an unmet need for suitable MRI based contrast agents which led to the development of several ultrasmall superparamagnetic iron oxide nanoparticles (USPIONs). USPIONs with a size of less than 50 nm showed promising MRI contrast ability, excellent biocompatibility and demonstrated great potential as a diagnostic tool for nanotheranostics [35].

In this study, modular two-in-one chitosan nano-cocktails containing both iron oxide and cerium oxide were developed for the treatment of inflammatory diseases. The nano-cocktails were designed to also allow the tracking of material delivery to the target site. Two different synthesis methods including electrostatic self-assembly (Chit-IOCO) and ionic gelation methods (Chit-TPP-IOCO) were employed. These synthesis approaches were chosen to allow ease of production, an important factor required for easy commercialisation and clinical translation. Cerium oxide nanoparticles (CO) and iron oxide nanoparticles (IO) were used as the treatment module and MRI imaging contrast agents respectively. Tripolyphosphate (TPP) was used as the crosslinker agents for chitosan gelation in the gelation method. We investigated the in vitro anti-inflammatory and MRI contrast ability of the nano-cocktails in RAW264.7 cells. Importantly, in vivo MRI contrast ability, anti-inflammatory and anti-fibrosis efficacy and biocompatibility of the nano-cocktails in CCl_4-induced liver inflammation mice model were

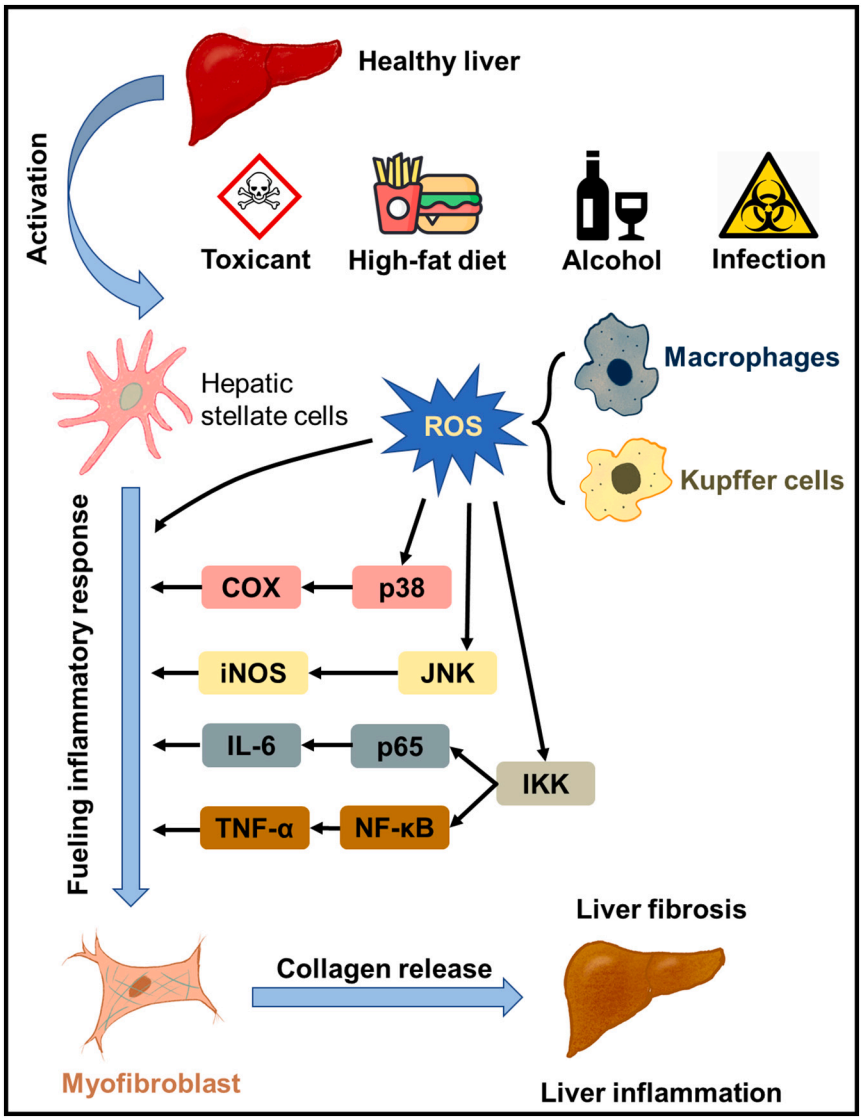

Fig. 1. Schematic representation of the progression of liver fibrosis and liver inflammation. Hepatic stellate cells are activated from its quiescent state when liver is effected by toxicant, high-fat diet, alcohol or infections. This triggers the recruitment and activation of leukocytes and Kupffer cells (stellate macrophages) to regulate the behaviour of stellate cells. These activated macrophages are characterised by the increased expression of reactive oxygen species (ROS) and proinflammatory cytokines. Specifically, ROS stimulates the secretion of cyclooxygenase (COX) through the p38 mitogen-activated protein kinase (p38) pathway. It can also increase the expression of inducible NO synthase (iNOS) through c-Jun N-terminal kinase (JNK) pathway. Additionally, tumor necrosis factor-α (TNF-α) and interleukin 6 (IL-6) are overexpressed by the 'inhibitor of nuclear factor-κB (IκB) kinase' (IKK) complex pathway. Subsequently, these pro inflammatory cytokines transfer the stellate cells to myofibroblasts. Collagen produced by myofibroblasts eventually cause liver fibrosis.

evaluated.

2. Methods

2.1. Materials

Iron (II) ammonium sulfate, hydrochloric acid (reagent grade, 37%), ammonium hydroxide solution (30% NH_4OH in H_2O), cerium nitrate hexahydrate, ammonium cerium nitrate, sodium acetate trihydrate, acetic acid, low molecular weight chitosan, tripolyphosphate (TPP), poly(acrylic acid) (PAA), lipopolysaccharides (LPS) were purchased from Sigma-Aldrich. Bovine serum albumin (BSA) was purchased from Bovogen Biologicals Pty Ltd. Trisodium citrate (TSC) was purchased from Chem-supply. Carbon tetrachloride (CCl_4) was purchased from AnalaR®. Virgin olive oil and fat free instant skim milk powder were purchased from local market Coles. Phosphate-buffered saline (PBS) was purchased from ThermoFisher Scientific. Tris (hydroxymethyl) aminomethane (Tris base), Triton X-100, sodium dodecyl sulfate (SDS), NaCl (sodium chloride), ethylenediaminetetraacetic acid (EDTA), sodium pyrophosphate decahydrate, sodium fluoride, sodium orthovanadate, Alanine Transaminase (ALT) Activity Assay kit, Bilirubin Assay Kit and Protease Inhibitor Cocktail were purchased from Sigma-Aldrich. Precision Plus Protein™ Kaleidoscope™ Prestained Protein Standards, 30% Acrylamide/Bis Solution, Immun-Blot Low Fluorescence PVDF Membrane, ammonium persulfate and tetramethyl ethylenediamine were purchased from Bio Rad. Anti-mouse IL-6, anti-mouse TNF-α, anti-mouse COX-2, anti-mouse iNOS and anti-mouse β-actin were purchased from Abcam.

2.2. Synthesis of the nano-cocktails

Iron oxide nanoparticles, cerium oxide nanoparticle, Chit-TPP, Chi-IOCO and Chit-TPP-IOCO were synthesised as described in our previous studies [9] and as below.

2.2.1. Synthesis of iron oxide nanoparticles

The IO-PAA nanoparticles were prepared by the co-precipitation method [26]. Briefly, 200 mg of PAA was dissolved in 50 ml of MilliQ water. The PAA solution was purged with nitrogen for 30 min and then heated at 130 °C to reflux using an oil bath. A mixture of 0.51 mM $FeCl_3{\cdot}6H_2O$ (0.1378 g) and 0.25 mM $(NH_4)_2Fe(SO_4)_2{\cdot}6H_2O$ (0.099 g) was dissolved in 1 ml of 37% concentrated HCl. The mixed solution was then quickly added into the hot PAA solution. After stirring for 5 min, 15 ml of 30% concentrated ammonia solution was added into the mixture, followed by refluxing the solution for two hours. The resulting solution was concentrated using a 50 K molecular weight cut-off Amicon filter (Millipore, Inc.). The concentrated solution was then dialysed against 5 L of water at pH 10 for one day and pH 7 for three days. The PAA-coated iron oxide NPs were collected and stored at 4 °C.

2.2.2. Synthesis of cerium oxide nanoparticles

Cerium oxide nanoparticles (*CONP*) were prepared by the co-precipitation method. $(NH_4)_2Ce(NO_3)_6$ (0.685 g) and CH3COONa (2.5 g) were dissolved in deionised water (17.5 ml) and then CH_3COOH (2.5 ml) was added to the solution. After stirring at room temperature for 1 h, the mixture was heated at 100 °C in an oil bath with condensation reflux for 2 h. Finally, yellow precipitates were separated by centrifugation (6000*g*) for 10 min, washed twice with deionised water then resuspended in 5 ml of H_2O.

The TSC coated cerium oxide nanoparticles (*CO-TSC*) were then prepared by mixing 100 mg of CONP with 0.1 M TSC in 15 ml of H_2O for 24 h. The stirred mixture was then filtered by 100 K molecular weight cut-off Amicon filter (Millipore, Inc.) at 10,000*g* for 1 min to remove the large agglomerates. The CO-TSC nanoparticles were stored in 0.1 M TSC solution before use. The nanoparticle solution was dialysed against water using 10k MWCO Snakeskin tube before further use and tests.

2.2.3. Synthesis of Chi-IOCO

Chit-IOCO nanoparticles were prepared via self-assembling between the positively charged chitosan and the negatively charged IO-PAA and CO-TSC nanoparticles. (Fig. S1) CO-TSC was firstly dialysed against 1 l of MilliQ water for 30 min. Then, a mixture solution (0.5 ml) of IO-PAA and CO-TSC was pumped (0.2 ml/min) into 4.5 ml of filtered (0.45 μm) chitosan (pH 4.8) to form the chitosan-IOCO nanoparticle. Different concentration of chitosan, IO-PAA and CO-TSC with different pumping speeds and incubation times was optimised to prepare the nanocomposite. The mixture was then centrifuged at 10,000*g* for 30 min followed by sonication for 5 min (cooling down on ice every 30 s of the sonication, 50% amplitude). Chit-IOCO nanoparticles were freeze- dried and the concentration was measured by the balance. Iron and cerium concentrations were measured by inductively coupled plasma optical emission spectrometry (ICP-OES).

2.2.4. Synthesis of chitosan-tripolyphosphate (Chit-TPP) nanoparticle

Chit-TPP nanoparticles were prepared via the ionic gelation method using tripolyphosphate (TPP) as the cross-linking reagent. Briefly, TPP (2.5 ml) was pumped (0.2 ml/min) into 5 ml of 0.1% (w/w) filtered (0.45 μm) chitosan (pH 4.8) to form the chit-TPP nanoparticle. Different concentrations of TPP and incubation times were used to optimise the nanoparticle. The mixture was then centrifuged at 10,000*g* for 30 min followed by sonication for total 5 min (cooling down on ice every 30 s of the sonication, 50% amplitude).

2.2.5. Synthesis of Chit-TPP-IOCO nanoparticle

Chit-TPP-IOCO nanoparticles were prepared via the ionic gelation method using IO-PAA, CO-TSC and tripolyphosphate (TPP) as the cross-linking reagents (Fig. S1). CO-TSC was firstly dialysed against 1 l of MilliQ water for 30 min. After that, a mixture solution (2.5 ml) of IO-PAA (0.15 mg), CO-TSC (0.15 mg) and TPP (3.15 mg) was pumped (0.2 ml/min) into 5 ml of 0.1% (w/w) filtered (0.45 μm) chitosan (pH 4.8) with continuously stirring for 1 h. The stirred mixture was then centrifuged at 10,000*g* for 30 min followed by sonication for 5 min (cooling down on ice every 30 s of the sonication, 50% amplitude). Chit-IOCO nanoparticles were freeze dried and the concentration was measured by the balance. Iron and cerium concentrations were measured by inductively coupled plasma optical emission spectrometry (ICP-OES).

2.3. Characterisations of the nanoparticles

Transmission electron microscopy (TEM) images were collected on a JEOL-JEM-1010 Transmission Electron Microscope operating at an accelerating voltage of 120 kV. The samples on the copper grid were stained with phosphotungstic acid (10 mg/ml, pH adjusted to 7.3 by sodium hydroxide) for 30s to visualise chitosan and the remaining acid solution was removed gently by a piece of tissue. The spectroscopy of iron and cerium in the nanoparticle was obtained via energy-dispersive X-ray spectrometry (EDS) coupled with scanning TEM at an accelerating voltage of 100 kV (JEOL-JEM-1010). EDS mapping images was scanned for 5 min. Iron and cerium concentrations were measured by inductively coupled plasma optical emission spectrometry (ICP-OES).

2.4. Biocompatibility of Chit-TPP, Chit-IOCO and Chit-TPP-IOCO nanoparticles - cytotoxicity study

Macrophage RAW 264.7 was attained from the American Type Culture Collection (ATCC). The cells were maintained in a non-treated 100 × 20 mm cell culture dish containing DMEM with fetal calf serum (10%), penicillin (100 U/ml) and L-glutamine (1%) and cultured in an incubator at 37 °C with 5% CO_2.

RAW 264.7 cells were detached by 2 ml of cold 1 × PBS when the cell confluence reached approximately 85%. Then cells were seeded into 96-well plate at a density of 10,000 cells/well. After 24 hour incubation, the

cells were treated with different concentrations of cerium in different nanoparticles Chit-IOCO, Chit-TPP and Chit-TPP-IOCO (Ce: 0, 0.1, 0.5, 1.0, 5.0, 10.0 and 20.0 μg/ml). After 24-hour nanoparticle treatment, cells were then treated with Calcein AM and Ethodium homodimer-1 fluorescence dye to detect live and dead macrophages. The fluorescence intensity was measured by EnSight™ Multimode Plate Reader (PerkinElmer) with an excitation wavelength of 494 nm and an emission wavelength of 517 nm for Calcein AM and Ex/Em = 528/617 nm for Ethodium homodimer-1. Cells treated with 0 μg/ml of nanoparticles were used as the positive control (100% of viability). Cells treated with 30% of methanol for 30 min were used as the negative control (0% of viability). Fluorescence images and bright-field images of macrophages were taken by Nikon ECLIPSE Ti2 fluorescence microscopy with Nikon Transmitted Light LED Lamphouse (TI2-D-LHLED) light source and CoolLED pE-4000 fluorescent light source. The fluorescence of 0 mg/ml sample was determined as 100% viability of the macrophages.

2.5. Haemocompatibility of Chit-IOCO and Chit-TPP-IOCO nanoparticles

270 μl of whole blood was treated with 30 μl of different concentrations of cerium in different nanoparticles Chit-IOCO and Chit-TPP-IOCO at pH 7.4. 1% Triton X-100 treated group was used as a positive control and PBS treated group was used as the negative control. After 1 hour incubation at 37 °C, the mixture solution was centrifuge at 14,000*g* for 20 min. The supernatant plasma was collected. The absorbance at 545 nm was measured by BMG LABTECH FLUOstar Omega. Images were taken by iPhone X.

2.6. Western blot analysis for in vitro assay

Macrophage RAW264.7 cells were seeded into 6-well plate at a density of 200,000 cells/well. After 48 h incubation, cells were separately treated with (1) cell culture medium, (2) 1 μg/ml of LPS, and (3) 1 μg/ml of LPS with the nanomaterials at different concentrations for 24 h. Cells were then lysed with lysis buffer for 15 min on ice followed and centrifuged at 10,600*g* for 10 min at 4 °C. The supernatant was collected, and the protein concentration was detected by the micro BCA assay kit. Around 30 μg of protein for each sample was mix with 5× protein loading buffer then denatured at 95 °C for 10 min followed by immediately added into 12.5% SDS-PAGE gel. After SDS-PAGE, the proteins were transferred to a Mini LF PVDF membrane. Membranes were then washed by 1 × TBST for 5 min (20 mM of Tris, 150 mM of NaCl, 0.1% (w/v) Tween® 20 detergent) (3 times) followed by blocking with 5% light milk (5 g in 100 ml of 1xTBST) for 1 h, and incubated overnight with primary antibody (against IL-6, TNF-α, COX-2, iNOS or β-actin) overnight at 4 °C. After incubation, membranes were then washed for 5 min by 1 × TBST (3 times) then incubated with secondary antibodies anti-rabbit HRP at room temperature for 1 h. After 3 times washing with 1 × TBST, the chemiluminescent images of LF PVDF membrane were taken by Bio-Rad ChemiDoc MP and Fujifilm LAS-3000. The gray values of chemiluminescence bands were analysed by ImageJ.

2.7. In vitro cell MRI

Macrophages RAW264.7 were seeded into a 6-well plate at a density of 300,000 cells/well. After 24 h incubation, cells were treated with Chit-IOCO or Chit-TPP-IOCO in cerium concentrations of 5 μg/ml and 10.0 μg/ml for 24 h. Subsequently, cells were washed with PBS for 3 times. The cells were then detached and centrifuged at 200*g* for 5 min. The cells were subsequently resuspended with 200 μL of warm 1% low-gelling temperature agarose and quickly transferred 50 μl into the prepared phantom vessel. T_2 values were calculated using 2D Multi slice multi echo (MSME) spin echo sequence using TR = 2630 ms, 32 echoes (5–160 ms), 0.117 × 0.117 mm in-plane resolution. The acquisition time was 11 min.

2.8. Animal study

Animal study was conducted at the University of Queensland (Brisbane, Australia). Care and use of laboratory animal followed the national guidelines and were approved by the institutional animal care and ethics committees of the University of Queensland. 6 weeks old C57BL/6 mice (Animal Resources Centre, ARC, Western Australia) were treated with Chit-IOCO via tail vein injection in three concentrations based on cerium (0 μg/10 g, 1 μg/10 g and 3 μg/10 g in PBS). Then C57BL/6 mice were treated with CCl_4 (5 μl/10 g, diluted to 10% in olive oil) twice a week for 4 weeks via intraperitoneal injection to induce liver fibrosis and liver inflammation. Olive oil-treated mice were used as baseline control. Mice were placed in 12 hour light/dark cycle, temperature at (30 ± 0.5) °C, and relative humidity of (55 ± 0.5) % and had free access to food and water. The weight of the animals was measured at day 1, 2, 6, 9, 13, 16, 20, 23, 28 after injection of the nano-cocktails.

2.9. In vivo MRI

Anaesthetised mice were placed in a preclinical MRI system, comprising a 300 mm bore 7 T ClinScan, running Siemens VB17. A 40 mm ID mouse body MRI rf coil was used to acquire the images. The following images were acquired.

1. Localiser images – Three orthogonal gradient echo images were acquired with the following parameters: TR = 23 msec, TE = 4.43 msec, field of view 100 × 100 mm, slice thickness = 1 mm, matrix = 256 × 256, flip angle = 25°, bandwidth = 260 Hz/Px, total scan time = 18 s.
2. 2D T_2 spin echo images – respiratory gated 2D spin echo image were acquired using the following parameters: TR = 1200, TE = 12.7, 25.4, 38.1, 50.8, 63.5 msec, concatenations = 2, field of view 30 × 30 mm, slice thickness = 1 mm, number of slices = 26, slice gap = 0 mm, image matrix = 128 × 128, resolution = 234 × 234 μm, flip angle = 90°, fat saturation enabled.
3. 2D T_2* gradient echo images – respiratory gated 2D gradient echo image were acquired using the following parameters: TR = 1000, TE = 4, 8, 16, 24 msec, concatenations = 8, field of view 35 × 35 mm, slice thickness = 1 mm, number of slices = 8, slice gap = 0 mm, image matrix = 128 × 128, resolution = 273 × 273 μm, flip angle = 20°, fat saturation enabled.

Relaxation time were determined from the T_2 and T_{2*} images automatically generated by the operating system. Region of interest (ROI) were placed in homogeneous regions of the liver away from major vessels and boundaries.

2.10. Organs and blood collection

Animals were euthanised at day 28 (the next day after the final injection of CCl_4). 700–800 μl of blood were collected by cardiac puncture. Blood was kept on ice for 30 min to allow clotting then centrifuged at 4000*g* for 30 min at 4 °C. 200 μl of supernatant serum was collected and stored at −20 °C for further test. ALT levels were detected by ALT activity assay kit and instructions followed as per manufacturer protocol. Total bilirubin level was measured by bilirubin assay kit as per manufacturer instructions. Liver, spleen, lung, kidney and heart organs were collected after the collection of blood. Liver for inflammatory cytokines analysis were weighed and homogenised for 5 min in lysis buffer on ice (lysis buffer: 20 mM Tris-HCl, 1% Triton X-100, 0.1% SDS, 50 mM NaCl, 2.5 mM EDTA, 1 mM $Na_4P_2O_7{\cdot}10\ H_2O$, 20 mM NaF, 1 mM Na_3VO_4, 1% (V/V) Protease Inhibitor Cocktail at pH 7.4). Organs were stored in 4% paraformaldehyde (PFA) solution for histology.

2.11. Western blot analysis for samples from in vivo study

The homogenised livers were centrifuged for 10 min at 4 °C. After that, bottom fragments of livers and top fatty layer were removed. Only middle layer of protein solution was collected for western blot. The protein concentration was detected by micro BCA assay kit. Around 100 μg of protein for each sample was mix with 5× protein loading buffer then denatured at 95 °C for 10 min followed by immediate addition into 12.5% SDS page. After SDS-PAGE, the cells were transferred to a Mini LF PVDF membrane.

Membranes were then washed by 1 × TBST (20 mM of Tris, 150 mM of NaCl, 0.1% (w/v) Tween® 20 detergent) for 3 times followed by blocking with 5% light milk (5 g in 100 ml of 1 × TBST) for 1 h, and incubated overnight with primary antibody (against IL-6, TNF-α, COX-2, iNOS or β-actin) at 4 °C. After overnight incubation, membranes were then washed by 1 × TBST (5 min) for 3 times then incubated with secondary antibodies (anti-rabbit HRP) at room temperature for 1 h. After which, wash with 1 × TBST (5 min) for 3 times. Chemiluminescence images of LF PVDF membrane were taken by Fujifilm LAS-3000. The gray value of chemiluminescence bands was analysed by ImageJ.

2.12. Histopathology

The organs were processed systemically for 9 h (70% of ethanol for 45 min, 90% of ethanol for 45 min, 95% of ethanol for 45 min, 100% of ethanol for 45 min (3 times), xylene for 30 min (3 times) and paraffin for 1 h (3 times)). After tissue processing, the samples were embedded in paraffin wax with the region of interest facing downwards. 4 μm sections were cut using a Leica RM2235 paraffin microtome and collected on to labelled SuperFrost Plus slides. Slides were submitted for haematoxylin and eosin staining on a Tissue-Tek Prisma autostainer, and coverslips added on the attached Tissue-Tek-Glas automated cover slipper. Histology images were taken by Leica DM IL LED inverted microscope with digital colour camera.

2.13. Statistical analysis of data

Data are presented as mean ± standard deviation (SD). One-way and two-way ANOVA was used in the analysis of significant difference. A p value ≤ 0.05 was considered significant. The graphs were plotted by GraphPad Prism 8.

3. Results and discussions

3.1. Synthesis and characterisation of the nano-cocktails

In this study, we synthesised chitosan nano-cocktails containing both iron oxide and cerium oxide (ceria) by two different methods and evaluated their functionalities. Chitosan, an amino polysaccharide obtained by alkaline deacetylation of natural abundant chitin [36], has been widely used for different applications such as cell culture [37] and drug carrier [38–40]. Here chitosan is employed to encapsulate both iron oxide and nanoceria.

Chit-IOCO nano-cocktails were synthesised by electrostatic self-assembly method via mixing the negatively charged IO-PAA and CO-TSC with the positively charged chitosan in solution (Fig. 2A). TEM image showed that Chit-IOCO nano-cocktails are around 60 nm in diameter (Fig. 2B). The spectroscopy of iron and cerium from Chit-IOCO was obtained via EDS together with scanning TEM (Fig. 2C). Both iron and cerium peaks were observed on the spectrum, indicating the presence of iron oxide nanoparticles and nanoceria in Chit-IOCO. EDS mapping of Chit-IOCO (Fig. 2D) illustrated that iron and cerium are evenly distributed in the nanoparticles. The mass ratio (around 7:3 by EDS and around 1:1 by ICP) of cerium and iron within the nano-cocktail

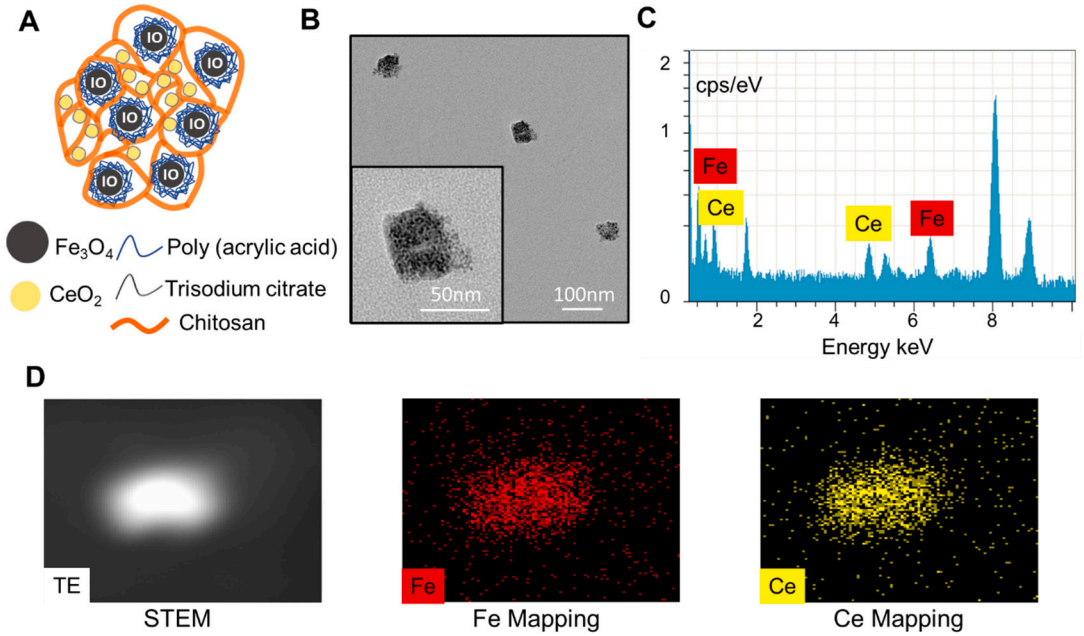

E

Element	Mass (%) by EDS	Atom(%) by EDS	Mass(%) by ICP
Cerium	68.36	46.27	52.37
Iron	31.64	53.73	47.63

Fig. 2. TEM and EDS analysis of Chit-IOCO. (A) Simulation structure of Chit-IOCO. (B) TEM image of Chit-IOCO. (C) EDS spectrum of the Chit-IOCO nanoparticles. (D) Scanning TEM (STEM), EDS iron (Fe) mapping and EDS cerium (Ce) mapping of the Chit-IOCO. (E) Mass % by EDS, Atom % by EDS and Mass % by ICP of iron and cerium in total amount of iron and cerium in Chit-IOCO.

was shown in Fig. 2E.

Chit-TPP-IOCO nano-cocktails were prepared by ionic gelation method. Tripolyphosphate (TPP) was used as a crosslinker for Chit-TPP-IOCO that encapsulated IO-PAA and CO-TSC within its network (Fig. 3A). Chit-TPP-IOCO with the length around 80 nm showed irregular shape under TEM (Fig. 3B). The spectroscopy of iron and cerium in the Chit-TPP-IOCO was obtained via EDS together with scanning TEM (Fig. 3C). The similar mass ratio (around 1:1) of cerium and iron within the nano-cocktail was founded in Chit-TPP-IOCO (Fig. 3E). Besides, both iron and cerium peaks were also observed on the spectrum, confirming the presence of iron oxide nanoparticles and nanoceria in Chit-TPP-IOCO. EDS mapping of Chit-TPP-IOCO (Fig. 3D) illustrated that iron and cerium are evenly distributed in the nanoparticles. However, the intensity of the EDS mapping of Chit-TPP-IOCO is not as strong as Chit-IOCO, indicating a higher loading of iron oxide and cerium oxide and a lower percentage of chitosan coating content in Chit-IOCO. The difference in the biocompatibility, anti-inflammatory ability and MRI contrast ability of these nano-cocktails with or without TPP will be investigated in the following studies.

3.2. Chit-IOCO and Chit-TPP-IOCO displayed no significant toxic effect on macrophages and red blood cells

RAW264.7 macrophages were incubated with different concentration of the nanoparticles for 24 h to test the cytotoxicity of the nano-cocktails on cells. Cells were then washed and subsequently treated with EthD-1 and Calcein AM. EthD-1 marked the dead macrophages nucleus with red fluorescence and Calcein AM showed green fluorescence by reacting with intracellular esterase in the live cells. The fluorescence intensity was measured by FLUOstar Omega plate reader (Fig. 4A(i), (ii)) and cell images were taken by fluorescence microscopy (Fig. 4A(iii)). A decrease in fluorescence intensity of Calcein AM indicated a lower cell number or a decrease in cell proliferation. It was found that Chit-IOCO had no significant effect on the proliferation of the cells at the concentrations of cerium from 0.1 μg/m to 10 μg/ml. At 20 μg/ml, Chit-IOCO significantly decreased the cell proliferation. Chit-TPP-IOCO, however, affected cell proliferation from a much lower concentration at 1 μg/ml of cerium. Interestingly, no cell death was detected by EthD-1 in all nano-cocktail-treated groups, demonstrated by similar fluorescence intensities of EthD1 in all conditions compared to non-treated cell control. Therefore, the results suggested that the nano-cocktails could inhibit the proliferation of macrophages without causing cell death. This characteristic can be an advantage as it could help control the proliferation of macrophages at the site of inflammation, thus control the development of inflammatory diseases.

The haemocompatibility of the nano-cocktails was investigated as they were designed as injectable nano-cocktails. Human whole blood was incubated with different nano-cocktails at different concentrations of cerium for 4 h. PBS-treated group was used as a negative control and 1% Triton-100X treated group was employed as a positive control. The absorbance of plasma at 545 nm was measured after centrifuging the samples at the end of the incubation. Fig. 4B(i), (ii) showed no haemolysis of human whole blood after treatment with either Chit-IOCO or Chit-TPP-IOCO. Similarly, Fig. 4B(iii) images indicated no colour changes in all of the nano-cocktails treated whole blood. Overall, these nano-cocktails showed no harmful effect on red blood cells.

3.3. Chit-IOCO and Chit-TPP-IOCO reduced inflammatory cytokines in LPS-stimulated macrophages

Tumor necrosis factor-α (TNF-α) [41], interleukin-6 (IL-6) [42] cyclooxygenase 2 isoform (COX-2) [43] and inducible nitric oxide synthase (iNOS) [44] are inflammatory cytokines that can be produced by immune cells, such as macrophages and Kupffer cells in the liver. In our studies, we employed RAW 264.7 as the cell model because it is one of the most common macrophage cell lines used for inflammation-related

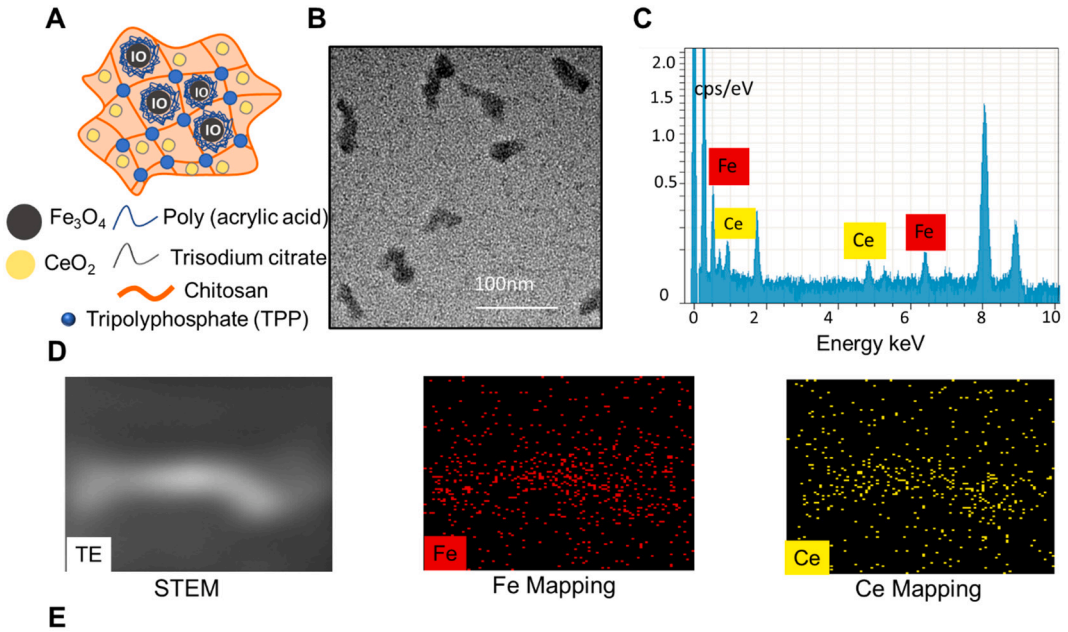

E

Element	Mass (%) by EDS	Atom(%) by EDS	Mass(%) by ICP
Cerium	53.90	31.78	53.50
Iron	46.10	68.22	46.50

Fig. 3. TEM and EDS analysis of Chit-TPP-IOCO. (A) Simulation structure of Chit-TPP-IOCO. (B) TEM image of Chit-TPP-IOCO. (C) EDS spectrum of the Chit-TPP-IOCO nanoparticles. (D) Scanning TEM (STEM), EDS iron (Fe) mapping and EDS cerium (Ce) mapping of the Chit-TPP-IOCO. (E) Mass % by EDS, Atom % by EDS and Mass % by ICP of iron and cerium in total amount of iron and cerium in Chit-TPP-IOCO.

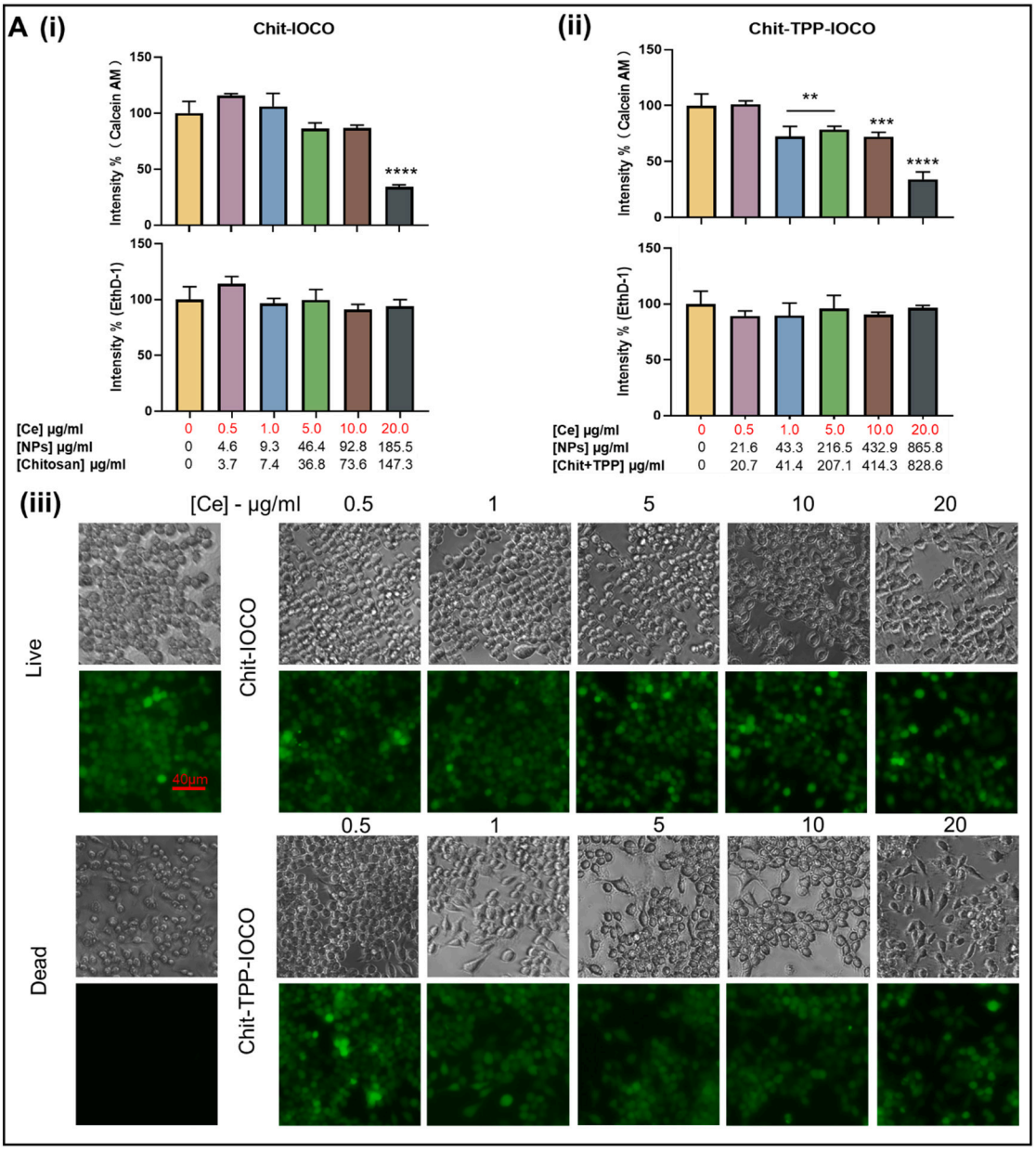

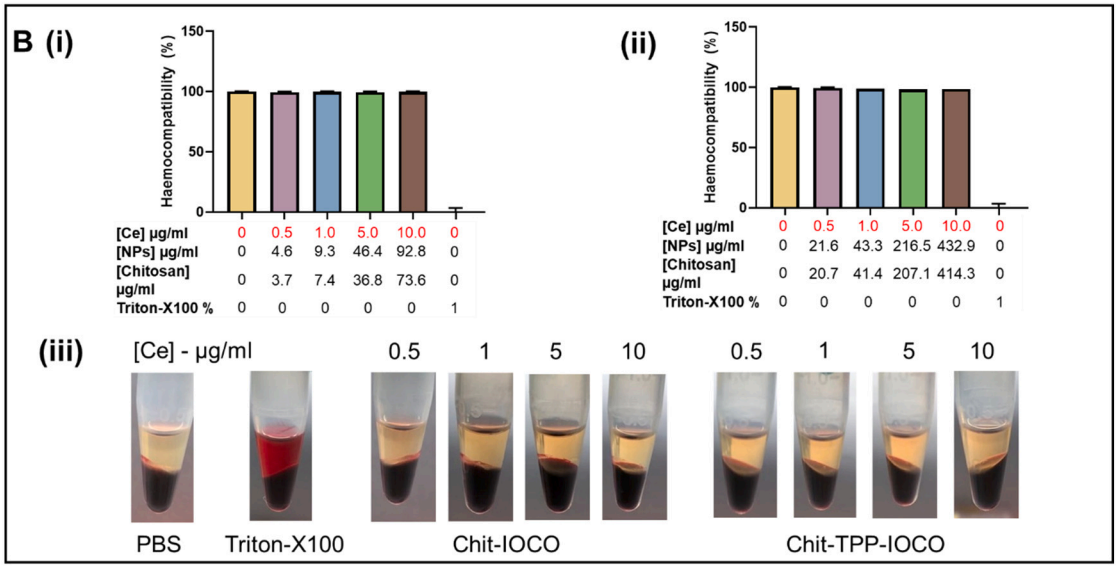

(caption on next page)

Fig. 4. In vitro biocompatibility of Chit-IOCO. (A) Cytotoxicity study of RAW 264.7 macrophages with Chit-IOCO and Chit-TPP-IOCO nanoparticles. RAW 264.7 macrophage was incubated with different nano-cocktails for 24 h. Cells viability was detected by LIVE/DEAD Cell Viability (Calcein AM/Ethidium homodimer-1). The fluorescence intensity was measured by PerkinElmer plate reader. The fluorescent image was taken by Nikon ECLIPSE Ti2 IX51 fluorescence microscopy. (i) The viability of the RAW 264.7 after 24 hour incubation with Chit-IOCO. (ii) The viability of the RAW 264.7 after 24 hour incubation with Chit-TPP-IOCO. (iii) Fluorescence images of the cells taken on the first day of the nanoparticle treatment. * Compared with cells only control: $^{**}p < 0.01$, $^{***}p < 0.001$, $^{****}p < 0.0001$ (B) Haemocompatibility of Chit-IOCO and Chit-TPP-IOCO nanoparticles. Human blood incubated with different nano-cocktails for 4 h. PBS was used as negative control and 1% of Triton-X100 was used as positive control. The absorbance of the plasma at 545 nm was measured by FLUOstar Omega plate reader. (i) The haemocompatibility of the Chit-IOCO. (ii) The haemocompatibility of the Chit-TPP-IOCO. (iii) Images of the plasma after treated with different nanoparticles. (For interpretation of the references to colour in this figure, the reader is referred to the web version of this article.)

diseases [45,46]. Currently, TNF-α is considered to be an important mediator of inflammation and apoptosis. High concentration of TNF-α may also induce tissue damage [47]. Besides, the secretion of COX-2 enzyme is mainly stimulated by mitogens and other pro-inflammatory cytokines in the inflammation microenvironment [43]. Therefore, the expression of COX-2 at the disease lesion can reflect the level of inflammation [48]. Additionally, the elevated levels of IL-6 in the serum of patients were observed in inflammation-related diseases [49]. Moreover, iNOS is produced by activated macrophages and excessive production can cause toxicity and inflammation to cells [44]. Hence, nanoparticles that inhibit these proteins have great potential for the treatment of many chronic inflammatory diseases.

In this part, RAW264 cells were treated with LPS (1 μg/ml), with or without nanoparticles (Chit-IOCO, Chit-TPP, Chit-TPP-IOCO) in different concentrations of cerium or chitosan to investigate whether nanoparticles have anti-inflammatory effect in macrophage cells. The expression of inflammatory related proteins, including TNF-α, COX-2, IL-6 and iNOS, were measured by western blot. Fig. 5A showed that Chit-IOCO significantly inhibited the expression of TNF-α at cerium concentrations from 0.5 μg/ml. Chit-IOCO with cerium concentration of 10 μg/ml demonstrated significant suppression (around 55%) of TNF-α secretion. Moreover, Chit-IOCO nanoparticles at the same concentration inhibited COX-2 expression by 25% (Fig. 5B). However, Chit-IOCO failed to inhibit IL-6 and iNOS production (Fig. 5C and D). In contrast, Chit-TPP-IOCO at a cerium concentration of 10 μg/ml substantially reduced IL-6 secretion by 50% (Fig. 5C). Nevertheless, Chit-TPP-IOCO had no significant effect on the reduction of TNF-α, COX-2 and iNOS proteins secretion (Fig. 5A, B and C). Also, Chit-TPP without loading of cerium oxide or iron oxide nanoparticles failed to inhibit the production of these four protein types (Fig. 5).

According to the above results, Chit-IOCO was able to reduce the expression of the TNF-α and COX-2. Chit-TPP-IOCO was capable for down-regulating IL-6. However, Chit-TPP was not able to decrease the expression of the above four inflammation-related proteins. The anti-inflammatory ability of these nano-cocktails would be contributed by the cerium oxide components.

The anti-inflammatory ability of cerium oxide had also been reported by other studies. Selvaraj et al. [50] showed that cerium oxide nanoparticles at the size of 140 nm reduced the overexpression of the inflammatory cytokines in LPS-stimulated RAW264.7. These nanoceria reduced approximately 20% of TNF-α, 20% of COX-2, 30% of IL-6 and 30% of iNOS protein expression in active macrophages at the cerium concentration of 7 μg/ml. Hirst et al. [51] also showed that cerium oxide nanoparticles inhibited the expression of iNOS (25%) in LPS/IFN-γ stimulated J774A.1 macrophages at a cerium concentration of 1.72 μg/ml. In our study, Chit-IOCO induced a notable down-regulation of TNF-α (55%) and COX-2 (25%) in LPS-stimulated RAW264.7 at the cerium concentration of 10 μg/ml. Chit-TPP-IOCO (10 μg/ml of cerium) induced around 50% reduction of the overexpressed IL-6. None of these nano-cocktails could inhibit the iNOS expression. Overall, these nano-cocktails were able to reduce the overexpression of the cytokines like TNF-α, COX-2 and IL-6. However, no inhibition on iNOS was observed. The reason why Chit-IOCO and Chit-TPP-IOCO showed different inhibition profile is not clear and will require further investigation. Besides, further anti-inflammatory experiments with primary cells such as Kupffer cells and monocyte-derived macrophages will help to understand the anti-inflammatory mechanism of these nano-cocktails.

3.4. Chit-IOCO showed better MRI contrast ability than Chit-TPP-IOCO in macrophages

Previously we found that Chit-IOCO and Chit-TPP-IOCO have transverse relaxivities (r_2) at 308 and 149 $mM^{-1}\,s^{-1}$, respectively [9]. In this study, we evaluated the imaging capabilities of these nano-cocktails in RAW264.7 macrophages. Macrophages play a critical role in the initiation and resolution of inflammation. They are involved in the regulation of many inflammation-related cytokines, such as TNF-a and interleukins [52]. They are recruited, accumulated largely at inflammatory lesions and considered as good diagnostic targets of inflammation [53]. As expected, RAW264.7 treated with Chit-IOCO showed a strong MRI T_2 effect at iron concentration of 29.6 μg/ml (Fig. S2A, C). At a similar iron concentration, macrophages treated with Chit-TPP-IOCO did not display higher relaxation rates than the non-treated group (Fig. S2B, D). These results clearly demonstrate that Chit-IOCO is more effective than Chit-TPP-IOCO as MRI contrast agents in macrophages.

According to the above results, Chit-IOCO nano-cocktails showed higher loading of cerium oxide and iron oxide nanoparticles than Chit-TPP-IOCO. Besides, anti-inflammatory studies indicated Chit-IOCO inhibited two cytokines (TNF-α and COX-2), while Chit-TPP-IOCO only inhibited the expression of IL-6 in LPS-stimulated macrophages. Importantly, Chit-IOCO has excellent MRI imaging capabilities in macrophages. However, no MRI T_2 signal was detected in Chit-TPP-IOCO treated macrophages. Overall, in vitro anti-inflammatory and MRI contrast ability showed that Chit-IOCO nano-cocktails could be established as a better candidate for the following in vivo studies.

3.5. Chit-IOCO displayed no significant effect on the weight, liver and other organs of C57BL/6

CCl_4-induced C57BL/6 mice are employed in our study since they are one of the most widely used liver fibrosis models that close to human [54–56]. C57BL/6 mice were administered with or without different concentrations of Chit-IOCO, followed by intraperitoneal (i.p) injection of CCl_4 or olive oil twice a week for four weeks. Mice weight was measured routinely before injections. No significant difference was observed in the weight changes in mice in different groups at day 27 (Fig. 6A(i), (ii)). In general, mice in all treatment and control groups displayed an increase in weight over time. (Fig. S3). No significant difference was observed in the weight of the livers between groups treated with different concentrations of nano-cocktail- and non-treated group.

Previous studies indicated that most chitosan nanoparticles (around 100 nm) were accumulated in the liver after 4 h of the injection [57,58]. Small amounts of chitosan nanoparticles were also found in spleen, kidneys, and lungs, heart and bone [59]. After degradation of the chitosan nanoparticles [60], the nanoceria and iron oxide nanoparticles could remain in the organs for weeks. A study showed that cerium oxide nanoparticles were mainly distributed to the liver and spleen, and a small amount of them was found in the kidneys and lungs. Another study also found that nanoceria could stay in the body for more than 5 weeks [61]. Similarly, iron oxide nanoparticles were also able to stay in the liver and spleen for more than 30 days [62,63]. Thus, it is necessary to investigate whether nanoceria could cause any damage to mice organs.

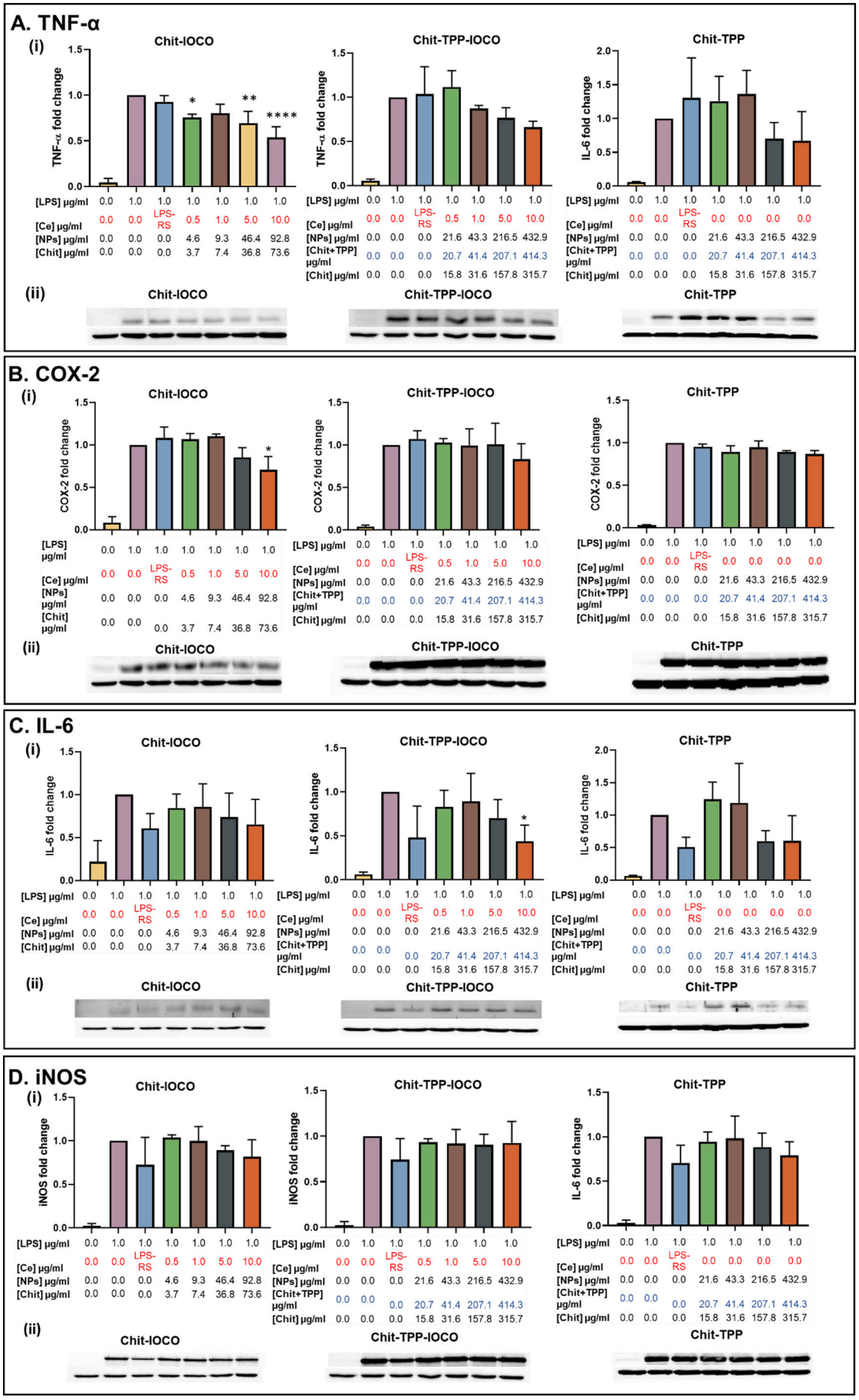

(caption on next page)

Fig. 5. Effect of Chit-IOCO, Chit-TPP-IOCO and Chit-TPP on the inflammatory protein secretion from LPS-stimulated macrophage RAW264 cells. (A) Effect of the nano-cocktails on the TNF-α protein secretion from LPS-stimulated macrophage RAW264 cells. (i) Graphs showing the TNF-α protein level of the cells treated with the nanomaterials in different concentrations of cerium or chitosan with the presence of LPS for 24 h. (ii) Chemiluminescent images of TNF-α protein and β-actin housekeeping protein. (B) Effect of the nano-cocktails on the LPS-stimulated COX-2 secretion from macrophage RAW264 cells. (i) Graphs showing the COX-2 protein level of the cells treated with the nanomaterials in different concentrations of cerium or chitosan with the presence of LPS for 24 h. (ii) Chemiluminescent images of COX-2 protein and β-actin housekeeping protein. (C) Effect of the nano-cocktails on the LPS-stimulated IL-6 secretion from macrophage RAW264 cells. (i) Graphs showing the IL-6 protein level of the cells treated with the nanomaterials in different concentrations of cerium or chitosan with the presence of LPS for 24 h. (ii) Chemiluminescent images of IL-6 protein and β-actin housekeeping protein. (D) Effect of the nano-cocktails on the LPS-stimulated iNOS secretion from macrophage RAW264 cells. (i) Graphs showing the iNOS protein level of the cells treated with the nanomaterials in different concentrations of cerium or chitosan with the presence of LPS for 24 h. (ii) Chemiluminescent images of iNOS protein and β-actin housekeeping protein. *Compare to LPS: $*p < 0.05$, $**p < 0.01$, $****p < 0.0001$.

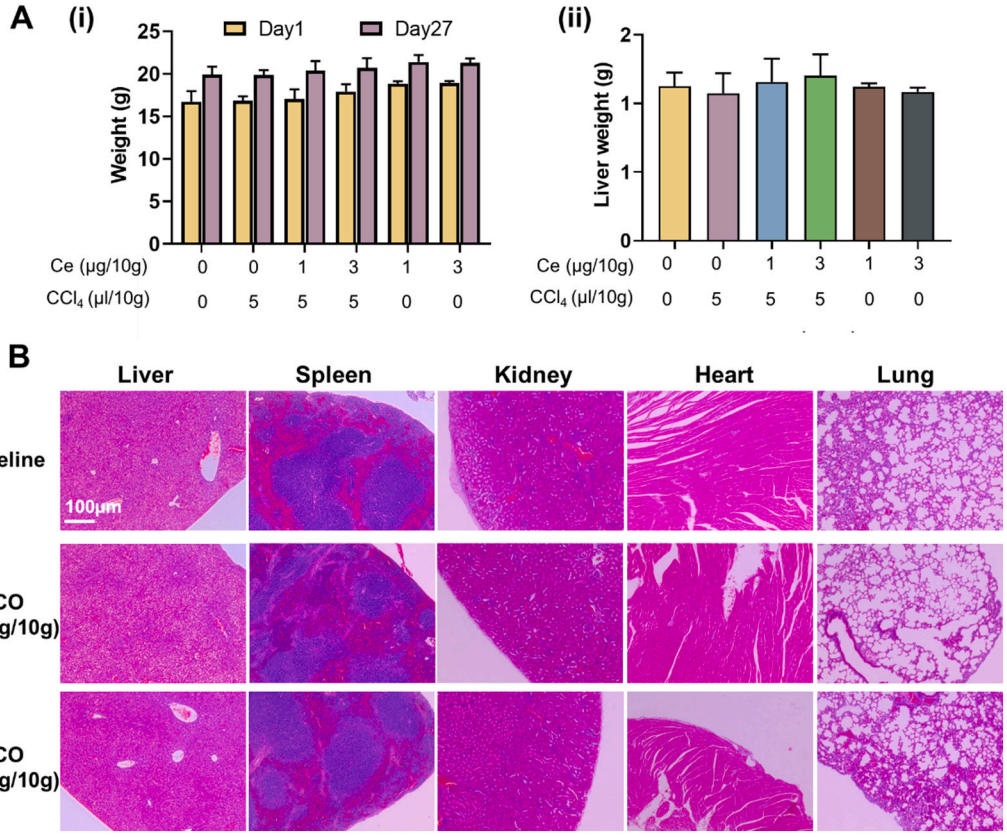

Fig. 6. Chit-IOCO displayed no significant effect on the weight, liver and other organs of C57BL/6. (A) Chit-IOCO displayed no significant effect on the weight of C57BL/6 mice and liver. Mice were treated with different concentrations of Chit-IOCO (cerium concentration: 0 μg/10 g, 1 μg/10 g and 3 μg/10 g). Olive oil injected C57BL/6 mice were used as negative control. Olive oil + CCl_4 injected mice were used as positive control. (i) Total weights of C57BL/6 mice at day 1 and day 27. (ii) Weight of livers of C57BL/6 mice at day 28. CCl_4-induced and healthy control groups: 6–7 mice per group, Chit-IOCO control groups: 3 mice per group. (B) Histology (haematoxylin–eosin staining) of organs at 28 days after administration of Chit-IOCO. Mice were treated with or without Chit-IOCO at different concentrations of cerium. At day 28, liver, spleen, kidney, heart and lung of each mice were collected and followed by H&E staining. The histopathology images were then taken by Leica DM IL LED inverted microscope using a 10× objective.

In our study, major organs (liver, spleen, kidney, heart and lung) were collected at day 28 after the administration of the Chit-IOCO. Thin sections were cut followed by staining with haematoxylin and eosin (H&E). Microscope images (Figs. 6B and S4) revealed no major difference between organs from control mice and Chit-IOCO treated mice. Also, no lesions were found in mice treated with different concentrations of Chit-IOCO.

Successful translation of materials to clinical applications depends on favorable biocompatibility. Overall, Chit-IOCO demonstrated no significant effect on the weight of C57BL/6 mice and liver. It also displayed good tolerance to both low and high concentrations of cerium.

3.6. Chit-IOCO decreased the inflammatory response in CCl4-induced C57BL/6 mice

Liver dysfunction elicits excessive total bilirubin (TBIL) and ALT levels in the blood [4,64]. It was reported that TBIL and active ALT levels were higher in the CCl_4 treated C57BL/6 than untreated mice [65]. In this haematological test, serum level of TBIL in CCl_4-induced C57BL/6 mice was overwhelmingly greater than the untreated-mice which signifies successful inflammation induction in the liver. TBIL level was successfully reduced to the basal level as observed in CCl_4 induced mice upon the injection of Chit-IOCO NPs (Fig. 7A(i)). In corroboration to our data, a recent study also indicated that TBIL levels was reduced upon injection of cerium oxide NPs at a cerium concentration of 0.82 μg/10 g and 1.62 μg/10 g in diethylnitrosamine (DEN) treated BALB/c mice [66]. No substantial increase of the active ALT was observed in CCl_4 induced mice in our study. Hence, in Chit-IOCO-treated mice, a significant decrease in ALT level was not detected (Fig. 7A(ii)). In addition, serum levels of TBIL and active ALT were not affected by the injection of Chit-IOCO NPs in healthy mice (not treated with CCl_4) which indicates good biocompatibility of our NPs at the therapeutic

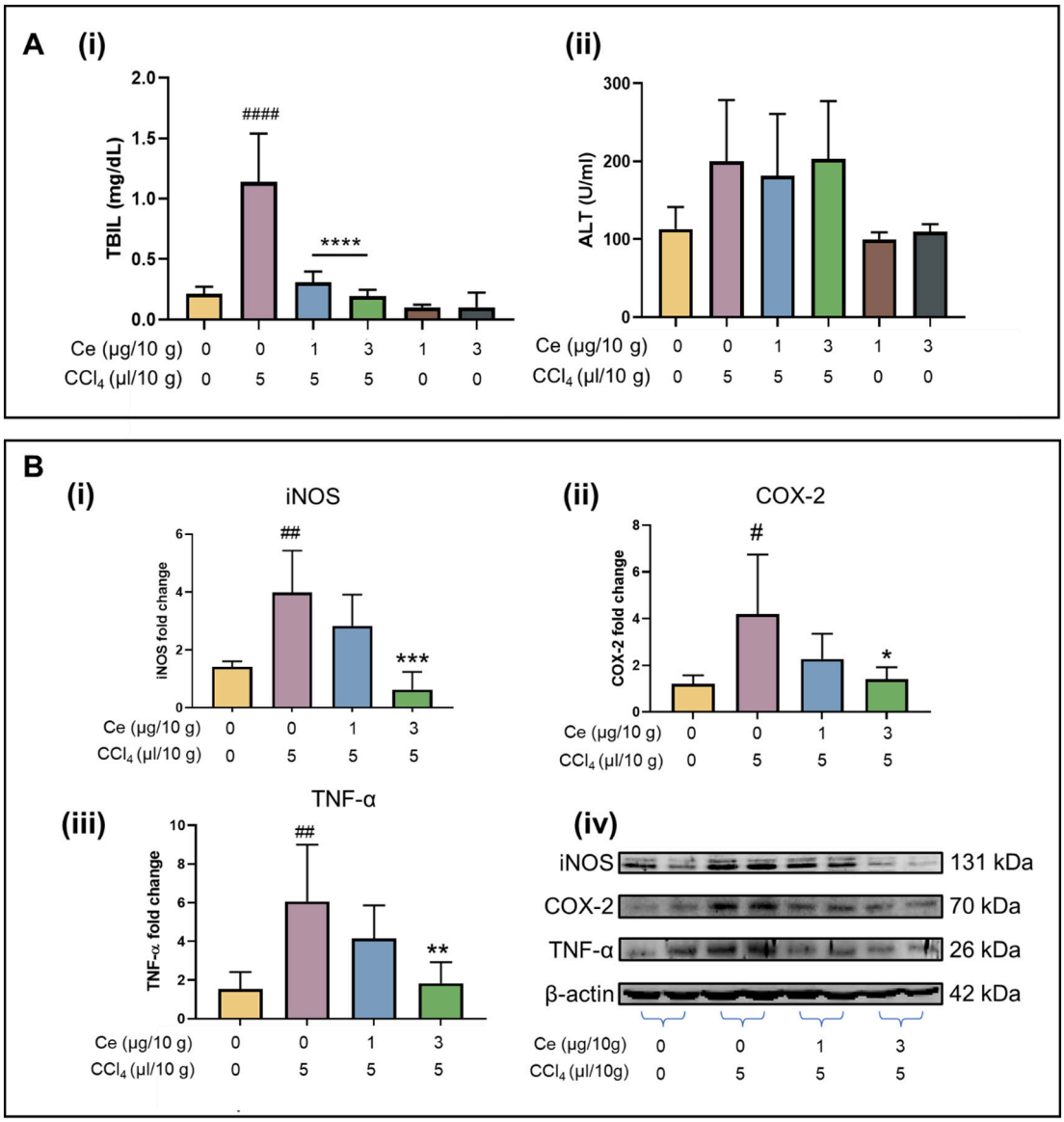

Fig. 7. Chit-IOCO decreased the inflammatory response in CCl_4-induced C57BL/6 mice. (A) Haematological analysis of blood from CCl_4 -induced inflammatory liver in C57BL/6. Mice were treated with different concentrations of Chit-IOCO (cerium concentration: 0 μg/10 g, 1 μg/10 g and 3 μg/10 g). Olive oil injected C57BL/6 mice were used as negative control. Olive oil + CCl_4 injected mice were used as positive control. Blood samples were collected at day 28 via cardiac puncture. Purified serum samples were used for the bilirubin (TBIL) and alanine transaminase (ALT) level test. (i) Serum levels of TBIL in C57BL/6 mice at day 28. (ii) ALT level in the serum of C57BL/6 mice at day 27. $\#\#\#\#p < 0.0001$ compare to baseline mice. ****$p < 0.0001$ compare to CCl_4 only-treated mice. CCl_4-induced groups and healthy control group: 6–7 mice per group, Chit-IOCO control groups: 3 mice per group. (B) Chit-IOCO decreases the overexpression of inflammatory proteins in CCl_4-induced C57BL/6 mice. The protein expression in the liver of C57BL/6 mice at day 28 was measured via western blot. (i), (ii), (iii) Graphs showing the iNOS, COX-2 and TNF-α protein levels normalised to β-actin, respectively. (iv) Images represent western blot for iNOS, COX-2, TNF-α and β-actin. $\#p < 0.05$, $\#\#p < 0.01$ compare to baseline mice, *$p < 0.05$, **$p < 0.01$, ***$p < 0.001$ compare to CCl_4 only-treated mice. $N = 5$–6 mice per group.

doses injected (Fig. 7A). However, administration of a much higher dose of cerium oxide could be toxic to the mice. A study on CD-1® mice showed that a high concentration of cerium oxide nanoparticle (16 mg/10 g) doubled the basal TBIL and ALT levels in normal mice [67]. Overall, haematological analysis indicated that these Chit-IOCO nano-cocktails successfully reduced the TBIL level in CCl_4 -induced C57BL/6 mice. Importantly, Chit-IOCO nano-cocktails at the therapeutic doses demonstrated excellent biocompatibility with no significant effects on basal TBIL and ALT levels.

As discussed earlier, TNF-α, iNOS, COX-2 and IL-6 proteins are involved in the development of hepatitis. During the progression of liver inflammation, many cytokines are released by ROS-stimulated macrophages, Kupffer cells and hepatic stellate cells [68]. IKK, JNK and p38, are three major signaling pathways that are involved in the production of inflammatory cytokines [69]. IKK complexes regulate the nuclear factor-κB (NF-κB) pathway to secrete the expression of the TNF-α. It is considered to be an important mediator of humoral immune response and apoptosis [41]. Additionally, p38/RelA pathway was required for the activation of IL-6 under the regulation of IKK complexes [70]. It has been reported that iNOS play an important role in regulation of fibrosis and sclerosis and JNK pathway is involved in regulation of iNOS expression [71]. Moreover, prostaglandin E2 (PGE2) secreted by COX-2 was regulated by the p38 pathway. The progression of the inflammation is affected by the level of PGE2. Hence, in this study, TNF -α, iNOS, COX-2 and IL-6 proteins were measured to assess the anti-inflammatory effects of these nano-cocktails. The expression levels of these proteins in the liver of C57BL/6 were measured by western blot analysis. As anticipated, Fig. 7B displayed an overexpression of TNF-α, iNOS and

COX-2 in CCl_4-treated than in control mice. Importantly, Chit-IOCO administration resulted in a decrease in the expression of TNF-α, iNOS and COX-2 proteins. Also, the protein expression decreased as the cerium concentrations increased from 1 to 3 μg/10 g (Fig. 7B(i), (ii), & (iii)). Chemiluminescence images of protein bands (Fig. 7B(iv)) displayed a reduction in protein expression of TNF-α, iNOS and COX-2 in liver of Chit-IOCO injected CCl_4-induced mice. As discussed earlier, these cytokines are involved in the inflammatory processes hence a decrease in protein expression of these cytokines is attributed to the anti-inflammatory ability of nanoceria in the nano-cocktails. Similarly, Oró et al. reported that cerium oxide nanoparticles inhibited the expression of the TNF-α, iNOS and COX-2 level in the liver of CCl_4-induced rats at a cerium concentration of 0.82 μg/10 g [14]. Interestingly, in our study CCl_4 treatment for 4 weeks did not result in an increase in IL-6 protein expression (Fig. S5). Therefore, a significant decrease of IL-6 protein expression was not observed in Chit-IOCO treatment group. In contrast, Tan et al. [72] showed an overexpression of IL-6 level (3-fold higher) in serum of CCl_4-induced C57BL/6 (5 μl/10 g, 6 weeks). Another study by Huang et al. also indicated that the IL-6 level in the liver of CCl_4-induced C57BL/6 (10 μl/10 g) was 3 times higher than healthy mice after 24 h treatment and returns to basal level after 5 days. Nonetheless, in our study, C57BL/6 mice might not be treated long enough (4 weeks) or the concentration (5 μl/10 g) of CCl_4 was not high enough to trigger an overexpression of IL-6.

The anti-inflammatory ability of cerium oxide is related to its anti-ROS ability as different signaling pathways of these inflammatory cytokines were regulated by ROS [73,74]. Both macrophage and Kupffer cells are involved in the inflammatory and fibrotic response [75]. A study demonstrated that administration of nanoceria ([Ce] 5 μg/10 g) reduced oxidative stress (malonaldehyde (MDA) level) in CCl_4-induced CD-1® mice [61]. Besides, it was also found that cerium oxide nanoparticle inhibited the TNF-α and MDA level in the blood of hypoxia-treated rabbits. Previously, we demonstrated that the developed nano-cocktails have anti-ROS capability [9]. In this study, the anti-inflammatory effect of ceria nanoparticles in liver of CCl_4-induced C57BL/6 mice was explored for the first time. Overall, our results indicated that Chit-IOCO NPs have great potential in the reduction of inflammation in the CCl_4-treated liver via downregulating the expression of TNF-α, iNOS and COX-2.

3.7. *In vivo MRI contrast ability of Chit-IOCO – it was possible to track the delivery of Chit-IOCO to the liver*

Ultrasmall superparamagnetic iron oxide nanoparticles (USPIONs) have been employed as MRI contrast agents with immense potential in the diagnosis of various diseases such as cancer and inflammatory diseases [31,76]. Previously reported studies with USPIONs displayed reduced toxicity and longer circulation time in comparison to gadolinium-based MRI contrast agent [77,78]. Besides, USPIONs have better MRI contrast efficiency than the commercial MRI contrast agent Feridex I.V.® [79]. In our study, IONPs at the size of 10 nm were utilised as MRI contrast agents in the newly developed Chi-IOCO to detect the delivery of the nano-cocktails to the liver of C57BL/6 mice. Chit-IOCO NPs at different doses were intravenously injected into mice. T_2 and T_2* MR images were acquired for the liver region of C57BL/6 mice. No significant difference was observed in the T_2 weighted relaxation time (Fig. S6) between pre- and 1-day post-injection of the Chit-IOCO NPs. However, the more sensitive T_2* weighted imaging showed a decreased T_2* relaxation time after injection of Chit-IOCO. In addition, the higher the injection dose of Chit-IOCO, the lower the T_2* relaxation time in the liver due to the higher concentration of Fe administrated in mice and thus accumulated in the liver (Fig. 8B). Also, the T_2* MR images acquired illustrated a stronger contrast in the liver of mice treated with the higher concentration of Chit-IOCO (Fig. 8A). These results indicate that it is possible to track the delivery of Chit-IOCO to the mouse livers.

A study by Rosales et al. reported that polymer coated iron oxide

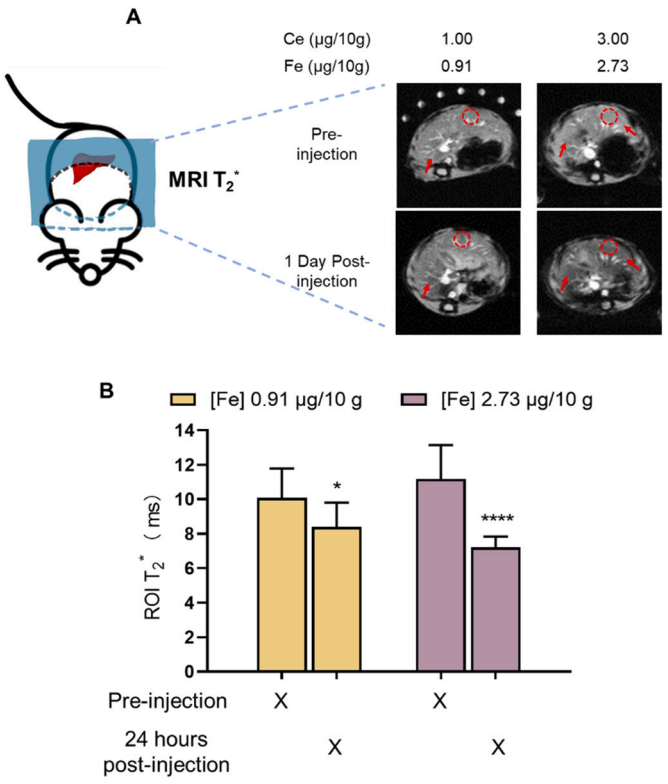

Fig. 8. In vivo MRI contrast ability of Chit-IOCO. Mice were treated with different concentrations of Chit-IOCO. MRI T_2* images were acquired before and after injection. (A) Graph showing the T_2* - weighted MRI images of mouse livers before and after one day post injection of Chit-IOCO at different concentrations of Fe. Red cycle showed typical ROI regions. For each mouse, T_2* at 3 different ROIs were measured and averaged. Red arrows showed the reduction of T_2* signal reduced by Chit-IOCO. (B) Graph showing liver T2* before and one day post injection of Chit-IOCO in different doses. Two-way ANOVA was used in the analysis of significant difference at region of interest (ROI) areas. $N = 5–6$ mice per group. (For interpretation of the references to colour in this figure legend, the reader is referred to the web version of this article.)

nanoparticles with a much higher iron concentration of 28 μg/10 g lowered the T_2* relaxation time from 3.3 ms to 1.2 ms in the liver of C57BL/6 mice 15 min post-injection [80]. Moreover, another study reported that glycyrrhetinic acid conjugated iron oxide (Fe_3O_4) nanoparticles with an iron concentration of 20 μg/10 g reduced T_2 relaxation time in mice liver 30 min after injection. However, T_2 relaxation time returned to basal level 7 h after injection [81]. In comparison to previously reported studies, the Chit-IOCO used here showed an effective T_2* contrast ability at very low iron concentrations of 0.91 μg/10 g and 2.73 μg/10 g. Importantly, the significant T_2* contrast was observed one day post-injection of Chit-IOCO NPs. Moreover, chronic liver injuries cause dilation and leakage of small blood vessels [82]. It will cause the enhanced permeability and retention effect in inflammatory liver diseases that enhance the nanoparticle distribution to the liver [83,84]. Overall, Chit-IOCO nano-cocktails showed outstanding potential as an MRI contrast agent.

3.8. *Chit-IOCO reduced liver fibrosis in CCl_4-treated C57BL/6 mice*

Fibrosis of the liver results from wound healing process that is usually caused by chronic liver diseases. Hepatitis is a typical example, whereby inflammation fuels the excessive secretion and accumulation of extracellular matrix (ECM) proteins of hepatic stellate cells and fibroblasts to form liver fibrosis [85]. Advanced liver fibrosis can also develop into cirrhosis, causing irreversible damage. In this animal model, toxic damage of liver caused by the injection of the CCl_4 and the

efficacy of NPs in improving liver fibrosis was assessed. Histopathology images showed clear fibrogenesis in the liver of CCl_4-treated mice receiving vehicle. (Figs. 9 and S7) Besides, large number of steatosis of hepatocytes can be discerned in the CCl_4-induced mice (black arrows). Typically, hepatocytes with steatosis have lipid drops accumulated in the surrounding cytoplasm and a centralised nucleus [86]. Fibrosis of liver and steatosis of hepatocytes were significantly reduced with the administration of Chit-IOCO. In addition, a further reduction in liver fibrosis lesions were observed in liver of mice treated with a higher nano-cocktail concentration (3 μg Ce/10 g) (Fig. 9). Chit IOCO displayed both a reduction in inflammation and fibrosis of liver in CCl_4 treated mice via a downregulation of inflammatory proteins in the liver. Overall, this is the first report demonstrating cerium oxide nanoparticle efficacy in reducing liver fibrosis in CCl_4-induced C57BL/6 mice.

4. Conclusion

In this study, in vitro toxicity studies showed that Chit-IOCO and Chit-TPP-IOCO inhibited the proliferation of macrophages without causing cell death. Both nano-cocktails are haemocompatible. In vitro anti-inflammatory study showed that Chit-IOCO could inhibit the overexpression of TNF-α, COX-2 while Chi-TPP-IOCO could reduce IL-6 production. Interestingly, MRI illustrated that Chit-IOCO is a better contrast agent than Chit-TPP-IOCO. Furthermore, in vivo MRI demonstrated that Chit-IOCO is also an effective contrast agent for MR imaging of the liver. Haematological analysis indicated that Chit-IOCO reduced TBIL levels, indicating less inflammation in CCl_4-induced mice treated with Chit-IOCO. Chit-IOCO displayed excellent anti-inflammatory capability by reducing the overexpression of TNF-α, iNOS and COX-2 in CCl_4 damaged liver. Moreover, histopathology images illustrated significant reduction of fibrotic areas upon administration of Chit-IOCO. Additionally, Chit-IOCO demonstrated good biocompatibility with no major difference of total body weight, liver weight, TBIL, ALT and histology images between blank vehicle and Chit-IOCO-treated mice. Besides, by conjugating with effective targeting ligands, Chit-IOCO could have the potential for other inflammatory diseases. For example, by employing specific antibody or peptide targeting vascular cell adhesion molecule 1 (VCAM-1) [87,88], a protein significantly expressed on atherosclerotic plaques, these nano-cocktails could be employed for theranostics of atherosclerosis.

To the best of our knowledge, this is the first study demonstrating the anti-inflammatory and anti-fibrosis capabilities of Chit-IOCO in the liver of CCl_4-induced C57BL/6 mice. Overall, our modular nano-cocktails displayed excellent potential for concurrent tracking of nanoparticle delivery and therapy of inflammatory diseases. The materials can also be employed as MRI contrast agent for the diagnosis of inflammatory diseases if they are labelled with appropriate targeting ligands. These promising results of our in vivo studies provide high possibility of translation of these nano-cocktails to clinical trials.

CRediT authorship contribution statement

Yuao Wu: Conceptualization, Investigation, Validation, Formal analysis, Visualization, Writing – Original Draft. **Gary Cowin**: Investigation, Visualization **Shehzahdi S. Moonshi**: Writing – Review & Editing, Investigation. **Huong D.N. Tran**: Investigation **Najma Fithri**: Investigation. **Andrew Whittaker**: Conceptualization, Writing – Review & Editing. **Run Zhang**: Conceptualization, Writing – Review & Editing. **Hang T. Ta**: Conceptualization, Writing – Review & Editing, Supervision, Resources, Project administration, Funding acquisition.

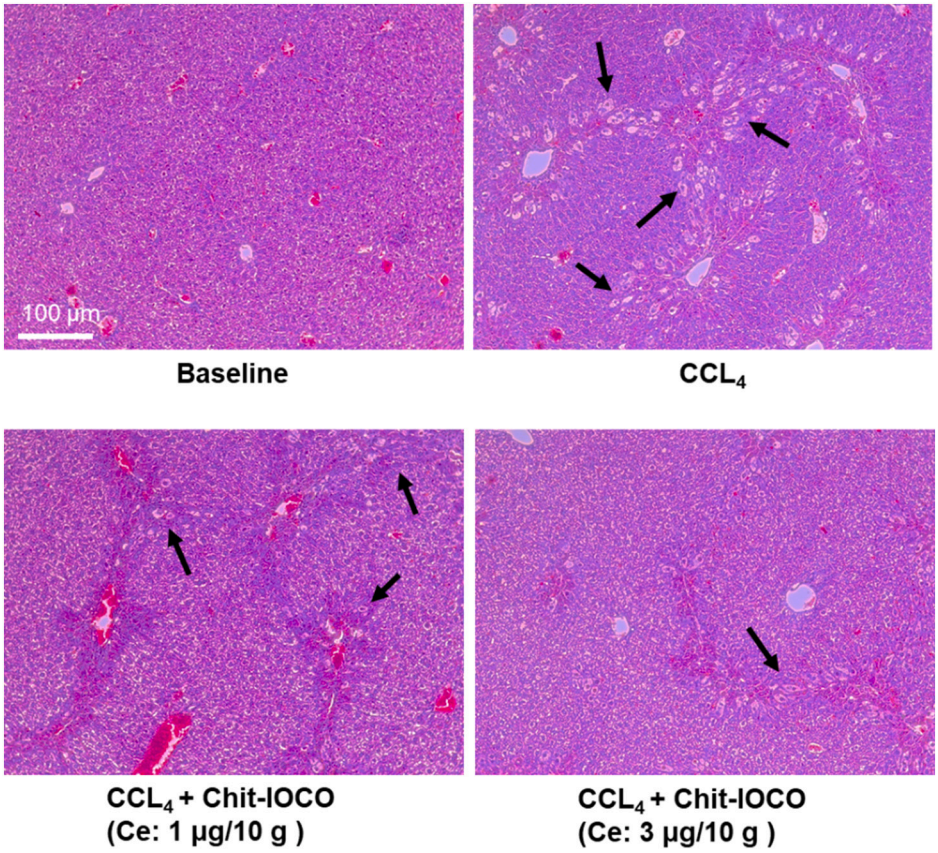

Fig. 9. Improvement of liver fibrosis at 28 days after the administration of different concentrations of Chit-IOCO. Mice were treated with or without CCl_4 and Chit-IOCO at different concentrations of cerium. At day 28, livers of each treatment groups were collected followed by H&E staining. The histopathology images were then taken by Leica DM IL LED inverted microscope using a 10× objective. Black arrows showed the position of micro-vesicular steatosis of hepatocytes.

Declaration of competing interest

The authors declare that they have no known competing financial interests or personal relationships that could have appeared to influence the work reported in this paper.

Acknowledgement

This work is funded by Australian National Health and Medical Research Council (HTT: APP1037310, APP1182347, APP2002827) and National Heart Foundation of Australia (HTT: 102761). The authors would like to acknowledge the Australian National Fabrication Facility (Queensland Node) and National Imaging Facility, Centre for Advanced Imaging for access to key items of equipment.

Appendix A. Supplementary data

Supplementary data to this article can be found online at https://doi.org/10.1016/j.msec.2021.112477.

References

[1] B. Mühlemann, T.C. Jones, P. de Barros Damgaard, M.E. Allentoft, I. Shevnina, A. Logvin, E. Usmanova, I.P. Panyushkina, B. Boldgiv, T. Bazartseren, Ancient hepatitis B viruses from the bronze age to the medieval period, Nature 557 (7705) (2018) 418–423.
[2] W.H. Organization, Global Hepatitis Report 2017, World Health Organization, 2017.
[3] X. Wang, J.R. Chowdhury, N.R. Chowdhury, Bilirubin metabolism: applied physiology, Curr. Paediatr. 16 (1) (2006) 70–74.
[4] N. Méndez-Sánchez, L. Vítek, N.E. Aguilar-Olivos, M. Uribe, Bilirubin as a biomarker in liver disease, in: V.B. Patel, V.R. Preedy (Eds.), Biomarkers in Liver Disease, Springer Netherlands, Dordrecht, 2017, pp. 281–304.
[5] S.D. Kershenobich, A. Weissbrod, Liver fibrosis and inflammation. A review, Ann. Hepatol. 2 (4) (2003) 159.
[6] A. Canbay, A.E. Feldstein, H. Higuchi, N. Werneburg, A. Grambihler, S.F. Bronk, G. J. Gores, Kupffer cell engulfment of apoptotic bodies stimulates death ligand and cytokine expression, Hepatology 38 (5) (2003) 1188–1198.
[7] H. Yang, Y. Xuefeng, W. Shandong, X. Jianhua, COX-2 in liver fibrosis, Clin. Chim. Acta 506 (2020) 196–203.
[8] R. Taub, Hepatoprotection via the IL-6/Stat3 pathway, J. Clin. Invest. 112 (7) (2003) 978–980.
[9] Y. Wu, R. Zhang, H.D.N. Tran, N.D. Kurniawan, S.S. Moonshi, A.K. Whittaker, H. T. Ta, Chitosan nano-cocktails containing both ceria and superparamagnetic iron oxide nanoparticles for reactive oxygen species-related theranostics, ACS Appl. Nano Mater. (2021), https://doi.org/10.1021/acsanm.1c00141.
[10] Y.A. Teterin, A.Y. Teterin, A. Lebedev, I. Utkin, The XPS spectra of cerium compounds containing oxygen, J. Electron Spectrosc. Relat. Phenom. 88 (1998) 275–279.
[11] D. Oró, T. Yudina, G. Fernández-Varo, E. Casals, V. Reichenbach, G. Casals, B.G. de la Presa, S. Sandalinas, S. Carvajal, V. Puntes, Cerium oxide nanoparticles reduce steatosis, portal hypertension and display anti-inflammatory properties in rats with liver fibrosis, J. Hepatol. 64 (3) (2016) 691–698.
[12] Y. Wu, H.T. Ta, Different approaches to synthesise cerium oxide nanoparticles and their corresponding physical characteristics, ROS scavenging and anti-inflammatory capabilities, J. Mater. Chem. B 9 (36) (2021) 7291–7301.
[13] K.A. Amin, M.S. Hassan, E.-S.T. Awad, K.S. Hashem, The protective effects of cerium oxide nanoparticles against hepatic oxidative damage induced by monocrotaline, Int. J. Nanomedicine 6 (2011) 143.
[14] H. Ta, Z. Li, C. Hagemeyer, G. Cowin, J. Palasubramaniam, K. Peter, A. Whittaker, Self-confirming molecular imaging of activated platelets via iron oxide nanoparticles displaying unique dual MRI contrast, Atherosclerosis 263 (2017), e146.
[15] H. Ta, S. Prabhu, E. Leitner, F. Jia, K. Putnam, N. Bassler, K. Peter, C. Hagemeyer, Targeted molecular imaging and cell homing in cardiovascular disease via antibody-sortagging, Atherosclerosis 241 (1) (2015), e26.
[16] H. Ta, S. Prabhu, E. Leitner, K. Putnam, F. Jia, N. Bassler, K. Peter, C. Hagemeyer, A novel biotechnological approach for targeted regenerative cell therapy and molecular imaging of atherothrombosis, Heart Lung Circ. 19 (2010) S10.
[17] H.T. Ta, N. Arndt, Y. Wu, H.J. Lim, S. Landeen, R. Zhang, D. Kamato, P.J. Little, A. K. Whittaker, Z.P. Xu, Activatable magnetic resonance nanosensor as a potential imaging agent for detecting and discriminating thrombosis, Nanoscale 10 (31) (2018) 15103–15115.
[18] H.T. Ta, Z. Li, C.E. Hagemeyer, G. Cowin, S. Zhang, J. Palasubramaniam, K. Alt, X. Wang, K. Peter, A.K. Whittaker, Molecular imaging of activated platelets via antibody-targeted ultra-small iron oxide nanoparticles displaying unique dual MRI contrast, Biomaterials 134 (2017) 31–42.
[19] H.T. Ta, Z. Li, Y. Wu, G. Cowin, S. Zhang, A. Yago, A.K. Whittaker, Z.P. Xu, Effects of magnetic field strength and particle aggregation on relaxivity of ultra-small dual contrast iron oxide nanoparticles, Mater. Res.Express 4 (11) (2017), 116105.
[20] H.T. Ta, S. Prabhu, E. Leitner, F. Jia, K. Putnam, N. Bassler, K. Peter, C. Hagemeyer, Antibody-sortagging: a universal approach towards targeted molecular imaging and cell homing in cardiovascular disease, Circ. Res. 107 (12) (2010) e37–e38.
[21] H.T. Ta, S. Prabhu, E. Leitner, F. Jia, D. von Elverfeldt, K.E. Jackson, T. Heidt, A.K. N. Nair, H. Pearce, C. Von Zur Muhlen, Enzymatic single-chain antibody tagging: a universal approach to targeted molecular imaging and cell homing in cardiovascular disease, Circ. Res. 109 (4) (2011) 365–373.
[22] K.X. Vazquez-Prada, J. Lam, D. Kamato, Z. Ping Xu, P.J. Little, H.T. Ta, Targeted molecular imaging of cardiovascular diseases by iron oxide nanoparticles, Arterioscler. Thromb. Vasc. Biol. 41 (2) (2020) 601–613. ATVBAHA. 120.315404.
[23] N.N.M. Yusof, A. McCann, P.J. Little, H.T. Ta, Non-invasive imaging techniques for the differentiation of acute and chronic thrombosis, Thromb. Res. 177 (2019) 161–171.
[24] Y. Zhang, A. Koradia, D. Kamato, A. Popat, P.J. Little, H.T. Ta, Treatment of atherosclerotic plaque: perspectives on theranostics, J. Pharm. Pharmacol. 71 (7) (2019) 1029–1043.
[25] A. Zia, Y. Wu, T. Nguyen, X. Wang, K. Peter, H.T. Ta, The choice of targets and ligands for site-specific delivery of nanomedicine to atherosclerosis, Cardiovasc. Res. 116 (13) (2020) 2055–2068.
[26] Y. Liu, Y. Wu, R. Zhang, J. Lam, J.C. Ng, Z.P. Xu, L. Li, H.T. Ta, Investigating the use of layered double hydroxide nanoparticles as carriers of metal oxides for theranostics of ROS-related diseases, ACS Appl. Bio Mater. 2 (12) (2019) 5930–5940.
[27] N. Arndt, H.D. Tran, R. Zhang, Z.P. Xu, H.T. Ta, Different approaches to develop nanosensors for diagnosis of diseases, Adv. Sci. 7 (24) (2020), 2001476.
[28] E. Gaston, J.F. Fraser, Z.P. Xu, H.T. Ta, Biology; medicine, nano-and micro-materials in the treatment of internal bleeding and uncontrolled hemorrhage, Nanomedicine 14 (2) (2018) 507–519.
[29] A.U. Rehman, Y. Wu, H.D. Tran, K. Vazquez-Prada, Y. Liu, H. Adelnia, N. D. Kurniawan, M.N. Anjum, S.S. Moonshi, H.T. Ta, Silver/iron oxide nano-popcorns for imaging and therapy, ACS Appl. Nano Mater. (2021). https://pubs.acs.org/action/showCitFormats?doi=10.1021/acsanm.1c01571&ref=pdf.
[30] Y. Wu, K.X. Vazquez-Prada, Y. Liu, A.K. Whittaker, R. Zhang, H.T. Ta, Recent advances in the development of theranostic nanoparticles for cardiovascular diseases, Nanotheranostics 5 (4) (2021) 499.
[31] S.M. Dadfar, K. Roemhild, N.I. Drude, S. von Stillfried, R. Knüchel, F. Kiessling, T. Lammers, Iron oxide nanoparticles: diagnostic, therapeutic and theranostic applications, Adv. Drug Deliv. Rev. 138 (2019) 302–325.
[32] Y.-X.J. Wang, Current status of superparamagnetic iron oxide contrast agents for liver magnetic resonance imaging, World J. Gastroenterol. 21 (47) (2015) 13400.
[33] S. Maurea, P.P. Mainenti, A. Tambasco, M. Imbriaco, C. Mollica, E. Laccetti, L. Camera, R. Liuzzi, M. Salvatore, Diagnostic accuracy of MR imaging to identify and characterize focal liver lesions: comparison between gadolinium and superparamagnetic iron oxide contrast media, Quant. Imaging Med. Surg. 4 (3) (2014) 181.
[34] A. Bjørnerud, L. Johansson, The utility of superparamagnetic contrast agents in MRI: theoretical consideration and applications in the cardiovascular system, NMR Biomed. 17 (7) (2004) 465–477.
[35] X. Zhao, H. Zhao, Z. Chen, M. Lan, Nanotechnology, Ultrasmall superparamagnetic iron oxide nanoparticles for magnetic resonance imaging contrast agent, J. Nanosci. Nanotechnol. 14 (1) (2014) 210–220.
[36] H.T. Ta, Light scattering for the masses: effect of heating on molecular weights of chitosan, in: LCGC Europe: solution for separation scientists, 2010, p. 27.
[37] F. Akther, P. Little, Z. Li, N.-T. Nguyen, H.T. Ta, Hydrogels as artificial matrices for cell seeding in microfluidic devices, RSC Adv. 10 (71) (2020) 43682–43703.
[38] H.T. Ta, C.R. Dass, I. Larson, P.F. Choong, D.E. Dunstan, A chitosan hydrogel delivery system for osteosarcoma gene therapy with pigment epithelium-derived factor combined with chemotherapy, Biomaterials 30 (27) (2009) 4815–4823.
[39] H.T. Ta, H. Han, I. Larson, C.R. Dass, D.E. Dunstan, Chitosan-dibasic orthophosphate hydrogel: a potential drug delivery system, Int. J. Pharm. 371 (1–2) (2009) 134–141.
[40] H.T. Ta, D.E. Dunstan, C.R. Dass, 21 anticancer activity and therapeutic applications of chitosan nanoparticles, in: S.-K. Kim (Ed.), Chitin, Chitosan, Oligosaccharides Their Derivatives: Biological Activities, CRC, 2010, pp. 271–284.
[41] K.B. Elkon, C.-C. Liu, J.G. Gall, J. Trevejo, M.W. Marino, K.A. Abrahamsen, X. Song, J.-L. Zhou, L.J. Old, R.G. Crystal, Tumor necrosis factor α plays a central role in immune-mediated clearance of adenoviral vectors, Proc. Natl. Acad. Sci. 94 (18) (1997) 9814–9819.
[42] J. Van Snick, Interleukin-6: an overview, Annu. Rev. Immunol. 8 (1) (1990) 253–278.
[43] K. Seibert, J. Masferrer, Role of inducible cyclooxygenase (COX-2) in inflammation, Receptor 4 (1) (1994) 17.
[44] L.S.F. Carvalho, N. Panzoldo, S.N. Santos, R. Modolo, B. Almeida, J.C.Q. e Silva, W. Nadruz-Jr, E.C. de Faria, A.C. Sposito, B.H.S. Group, HDL levels and oxidizability during myocardial infarction are associated with reduced endothelial-mediated vasodilation and nitric oxide bioavailability, Atherosclerosis 237 (2) (2014) 840–846.
[45] W. Yoo, J. Lee, K.H. Noh, S. Lee, D. Jung, M.H. Kabir, D. Park, C. Lee, K.-S. Kwon, J.-S. Kim, Progranulin attenuates liver fibrosis by downregulating the inflammatory response, Cell Death Dis. 10 (10) (2019) 1–12.
[46] C.-K. Tseng, C.-K. Lin, H.-W. Chang, Y.-H. Wu, F.-L. Yen, F.-R. Chang, W.-C. Chen, C.-C. Yeh, J.-C. Lee, Aqueous extract of gracilaria tenuistipitata suppresses LPS-induced NF-κB and MAPK activation in RAW 264.7 and rat peritoneal macrophages

and exerts hepatoprotective effects on carbon tetrachloride-treated rat, PLoS One 9 (1) (2014), e86557.
[47] F. Barone, B. Arvin, R. White, A. Miller, C. Webb, R. Willette, P. Lysko, G. Feuerstein, Tumor necrosis factor-α: a mediator of focal ischemic brain injury, Stroke 28 (6) (1997) 1233–1244.
[48] R. Rajakariar, M.M. Yaqoob, D.W. Gilroy, COX-2 in inflammation and resolution, Mol. Interv. 6 (4) (2006) 199.
[49] T. Tanaka, M. Narazaki, T. Kishimoto, IL-6 in inflammation, immunity, and disease, Cold Spring Harb. Perspect. Biol. 6 (10) (2014), a016295.
[50] V. Selvaraj, N.D. Manne, R. Arvapalli, K.M. Rice, G. Nandyala, E. Fankenhanel, E. R. Blough, Effect of cerium oxide nanoparticles on sepsis induced mortality and NF-κB signaling in cultured macrophages, Nanomedicine (London, England) 10 (8) (2015) 1275–1288.
[51] S.M. Hirst, A.S. Karakoti, R.D. Tyler, N. Sriranganathan, S. Seal, C.M. Reilly, Anti-inflammatory properties of cerium oxide nanoparticles, Small 5 (24) (2009) 2848–2856.
[52] N. Fujiwara, K. Kobayashi, Macrophages in inflammation, Curr. Drug Targets Inflamm. Allergy 4 (3) (2005) 281–286.
[53] M.F. Linton, S. Fazio, Macrophages, inflammation, and atherosclerosis, Int. J. Obes. 27 (3) (2003) S35–S40.
[54] S.C. Yanguas, B. Cogliati, J. Willebrords, M. Maes, I. Colle, B. Van den Bossche, C.P. M.S. de Oliveira, W. Andraus, V.A. Alves, I. Leclercq, Experimental models of liver fibrosis, Arch. Toxicol. 90 (5) (2016) 1025–1048.
[55] L.W. Weber, M. Boll, A. Stampfl, Hepatotoxicity and mechanism of action of haloalkanes: carbon tetrachloride as a toxicological model, Crit. Rev. Toxicol. 33 (2) (2003) 105–136.
[56] S. Basu, Carbon tetrachloride-induced lipid peroxidation: eicosanoid formation and their regulation by antioxidant nutrients, Toxicology 189 (1–2) (2003) 113–127.
[57] D. Sonin, E. Pochkaeva, S. Zhuravskii, V. Postnov, D. Korolev, L. Vasina, D. Kostina, D. Mukhametdinova, I. Zelinskaya, Y. Skorik, Biological safety and biodistribution of chitosan nanoparticles, Nanomaterials 10 (4) (2020) 810.
[58] S.W. Richardson, H.J. Kolbe, R. Duncan, Potential of low molecular mass chitosan as a DNA delivery system: biocompatibility, body distribution and ability to complex and protect DNA, Int. J. Pharm. 178 (2) (1999) 231–243.
[59] T. Banerjee, S. Mitra, A.K. Singh, R.K. Sharma, A. Maitra, Preparation, characterization and biodistribution of ultrafine chitosan nanoparticles, Int. J. Pharm. 243 (1–2) (2002) 93–105.
[60] N. Islam, I. Dmour, M.O. Taha, Degradability of chitosan micro/nanoparticles for pulmonary drug delivery, Heliyon 5 (5) (2019), e01684.
[61] S.M. Hirst, A. Karakoti, S. Singh, W. Self, R. Tyler, S. Seal, C.M. Reilly, Bio-distribution and in vivo antioxidant effects of cerium oxide nanoparticles in mice, Environ. Toxicol. 28 (2) (2013) 107–118.
[62] L. Lartigue, D. Alloyeau, J. Kolosnjaj-Tabi, Y. Javed, P. Guardia, A. Riedinger, C. Péchoux, T. Pellegrino, C. Wilhelm, F. Gazeau, Biodegradation of iron oxide nanocubes: high-resolution in situ monitoring, ACS Nano 7 (5) (2013) 3939–3952.
[63] H. Arami, A. Khandhar, D. Liggitt, K.M. Krishnan, In vivo delivery, pharmacokinetics, biodistribution and toxicity of iron oxide nanoparticles, Chem. Soc. Rev. 44 (23) (2015) 8576–8607.
[64] W.R. Kim, S.L. Flamm, A.M. Di Bisceglie, H.C. Bodenheimer, Serum activity of alanine aminotransferase (ALT) as an indicator of health and disease, Hepatology 47 (4) (2008) 1363–1370.
[65] M. Charbonneau, J. Brodeur, P. du Souich, G.L. Plaa, Correlation between acetone-potentiated CCl4-induced liver injury and blood concentrations after inhalation or oral administration, Toxicol. Appl. Pharmacol. 84 (2) (1986) 286–294.
[66] O.A. Adebayo, O. Akinloye, O.A. Adaramoye, Cerium oxide nanoparticles attenuate oxidative stress and inflammation in the liver of diethylnitrosamine-treated mice, Biol. Trace Elem. Res. 193 (1) (2020) 214–225.
[67] A. Poma, A.M. Ragnelli, J. de Lapuente, D. Ramos, M. Borras, P. Aimola, M. Di Gioacchino, S. Santucci, L. De Marzi, In vivo inflammatory effects of ceria nanoparticles on CD-1 mouse: evaluation by hematological, histological, and TEM analysis, J Immunol Res 2014 (2014).
[68] T. Fujita, S. Narumiya, Roles of hepatic stellate cells in liver inflammation: a new perspective, Inflamm. Regen. 36 (1) (2016) 1–6.
[69] H. Nakagawa, S. Maeda, Inflammation-and stress-related signaling pathways in hepatocarcinogenesis, World J. Gastroenterol. 18 (31) (2012) 4071.
[70] A.R. Brasier, The nuclear factor-κB–interleukin-6 signalling pathway mediating vascular inflammation, Cardiovasc. Res. 86 (2) (2010) 211–218.
[71] A. Lahti, U. Jalonen, H. Kankaanranta, E. Moilanen, C-Jun NH2-terminal kinase inhibitor anthra (1, 9-cd) pyrazol-6 (2H)-one reduces inducible nitric-oxide synthase expression by destabilizing mRNA in activated macrophages, Mol. Pharmacol. 64 (2) (2003) 308–315.
[72] H. Tan, Q. He, R. Li, F. Lei, X. Lei, Trillin reduces liver chronic inflammation and fibrosis in carbon tetrachloride (CCl4) induced liver injury in mice, Immunol. Investig. 45 (5) (2016) 371–382.
[73] M. Mittal, M.R. Siddiqui, K. Tran, S.P. Reddy, A.B. Malik, Reactive oxygen species in inflammation and tissue injury, Antioxid. Redox Signal. 20 (7) (2014) 1126–1167.
[74] S.J. Forrester, D.S. Kikuchi, M.S. Hernandes, Q. Xu, K.K. Griendling, Reactive oxygen species in metabolic and inflammatory signaling, Circ. Res. 122 (6) (2018) 877–902.
[75] F. Tacke, H.W. Zimmermann, Macrophage heterogeneity in liver injury and fibrosis, J. Hepatol. 60 (5) (2014) 1090–1096.
[76] M. Michalska, L. Machtoub, H.D. Manthey, E. Bauer, V. Herold, G. Krohne, G. Lykowsky, M. Hildenbrand, T. Kampf, P. Jakob, A. Zernecke, W.R. Bauer, Visualization of vascular inflammation in the atherosclerotic mouse by ultrasmall superparamagnetic iron oxide vascular cell adhesion molecule-1-specific nanoparticles, Arterioscler. Thromb. Vasc. Biol. 32 (10) (2012) 2350.
[77] H. Jung, B. Park, C. Lee, J. Cho, J. Suh, J. Park, Y. Kim, J. Kim, G. Cho, H. Cho, Dual MRI T1 and T2 (*) contrast with size-controlled iron oxide nanoparticles, Nanomedicine 10 (8) (2014) 1679–1689.
[78] Q. Wang, M. Shen, T. Zhao, Y. Xu, J. Lin, Y. Duan, H. Gu, Low toxicity and long circulation time of polyampholyte-coated magnetic nanoparticles for blood pool contrast agents, Sci. Rep. 5 (2015) 7774.
[79] J. Huang, L. Bu, J. Xie, K. Chen, Z. Cheng, X. Li, X. Chen, Effects of nanoparticle size on cellular uptake and liver MRI with polyvinylpyrrolidone-coated iron oxide nanoparticles, ACS Nano 4 (12) (2010) 7151–7160.
[80] Torres Martin, R. de Rosales, R. Tavaré, A. Glaria, G. Varma, A. Protti, P.J. Blower, 99mTc-bisphosphonate-iron oxide nanoparticle conjugates for dual-modality biomedical imaging, Bioconjug. Chem. 22 (3) (2011) 455–465.
[81] J. Li, R. Cha, Y. Zhang, H. Guo, K. Long, P. Gao, X. Wang, F. Zhou, X. Jiang, Iron oxide nanoparticles for targeted imaging of liver tumors with ultralow hepatotoxicity, J. Mater. Chem. B 6 (40) (2018) 6413–6423.
[82] R. Bataller, D.A. Brenner, Liver fibrosis, J. Clin. Invest. 115 (2) (2005) 209–218.
[83] Y. Liu, D. Sun, Q. Fan, Q. Ma, Z. Dong, W. Tao, H. Tao, Z. Liu, C. Wang, The enhanced permeability and retention effect based nanomedicine at the site of injury, Nano Res. 13 (2) (2020) 564–569.
[84] H. Nehoff, N.N. Parayath, L. Domanovitch, S. Taurin, K. Greish, Nanomedicine for drug targeting: strategies beyond the enhanced permeability and retention effect, Int. J. Nanomedicine 9 (2014) 2539.
[85] S.L. Friedman, Liver fibrosis–from bench to bedside, J. Hepatol. 38 (2003) 38–53.
[86] E.M. Brunt, B.A. Neuschwander-Tetri, A.D. Burt, in: A. Burt, B. Portmann, L. Ferrell (Eds.), Fatty Liver Disease: Alcoholic and Nonalcoholic, 6th ed., 2011, pp. 293–359.
[87] S. Kinlay, J. Egido, Inflammatory biomarkers in stable atherosclerosis, Am. J. Cardiol. 98 (11) (2006) S2–S8.
[88] A.-M. Kampoli, D. Tousoulis, C. Antoniades, G. Siasos, C. Stefanadis, Biomarkers of premature atherosclerosis, Trends Mol. Med. 15 (7) (2009) 323–332.

Supplementary Information for

Engineering Chitosan Nano-Cocktail Containing Iron Oxide and Ceria: A Two-in-One Approach for Treatment of Inflammatory Diseases and Tracking of Material Delivery

Yuao Wu[1,2], Gary Cowin[4], Shehzahdi S. Moonshi[1], Huong D.N. Tran[1,2], Najma Annuria Fithri[1], Andrew Whittaker[2,5], Run Zhang[2], Hang T. Ta[1,2,3,*]

[1]Queensland Micro- and Nanotechnology Centre, Griffith University, Brisbane, 4111, Australia

[2]Australian Institute for Bioengineering and Nanotechnology, University of Queensland, Brisbane, 4072, Australia

[3]School of Environment and Science, Griffith University, Brisbane, 4111, Australia

[4]Centre of Advanced Imaging, University of Queensland, Brisbane, 4072, Australia

[5]ARC Centre of Excellence in Convergent Bio-Nano Science and Technology, The University of Queensland, Brisbane, QLD 4072, Australia

*Correspondence to Hang T. Ta (h.ta@griffith.edu.au)

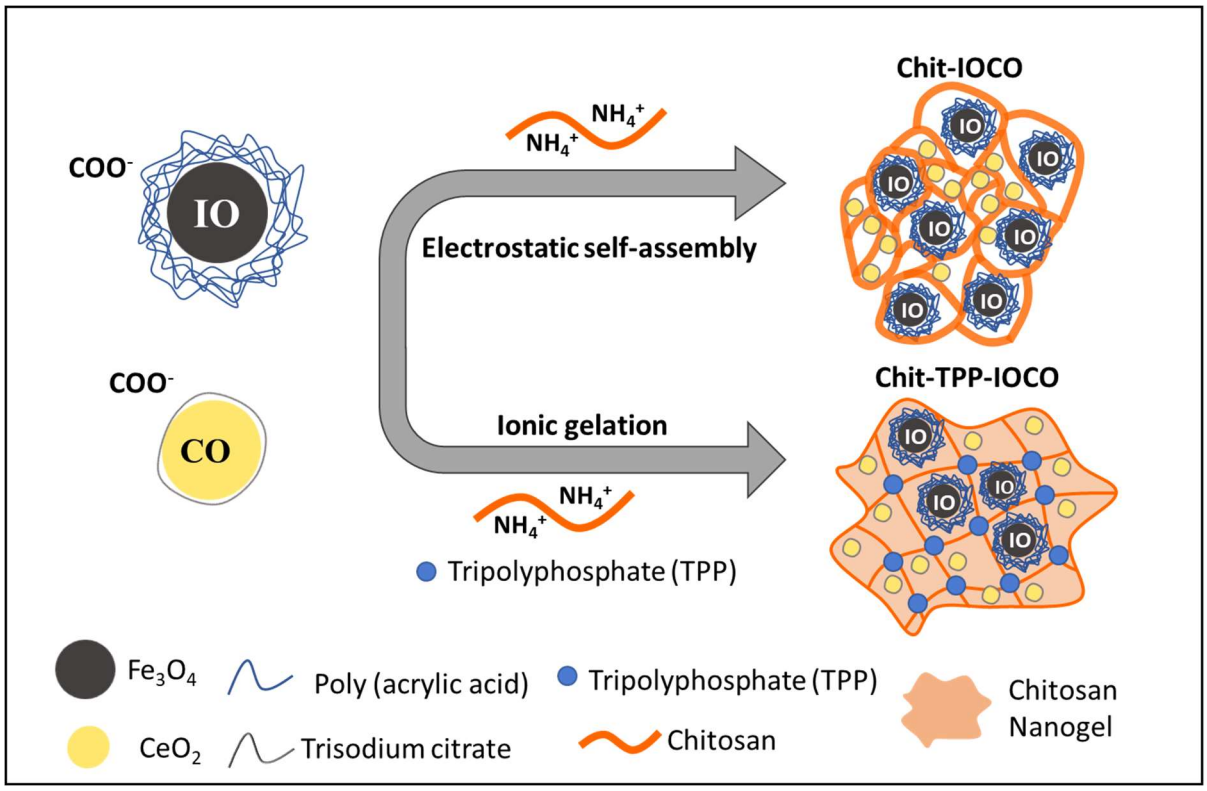

Fig S1. Image illustrating the synthesis of Chit-IOCO and Chit-TPP-IOCO. (1) Chit-IOCO nanoparticles were prepared via the electrostatic self-assembly method between the positively charged chitosan and the negatively charged IO-PAA and CO-TSC. CO-TSC was firstly dialysed against 1 l of milliQ water for 30 min. Then, a mixture solution (0.5 ml) of IO-PAA and CO-TSC was pumped (0.2 ml/min) into 4.5 ml of filtered (0.45 µm) chitosan (pH 4.8) to form the chitosan-IOCO nanoparticle.
(2) Chit-TPP-IOCO nanoparticles were prepared via the ionic gelation method between chitosan and tripolyphosphate (TPP) (a cross-linking reagent), which encapsulates IO-PAA and CO-TSC within their nanogel structure. CO-TSC was firstly dialysed against 1 L of milliQ water for 30min. After that, a mixture solution (2.5 ml) of IO-PAA (0.15 mg), CO-TSC (0.15 mg) and TPP (3.15 mg) was pumped (0.2 ml/min) in 5 ml of 0.1% (w/w) filtered (0.45 µm) chitosan (pH 4.8) with continuously string for 1 hour to form the chitosan-TPP-IOCO nanoparticle.

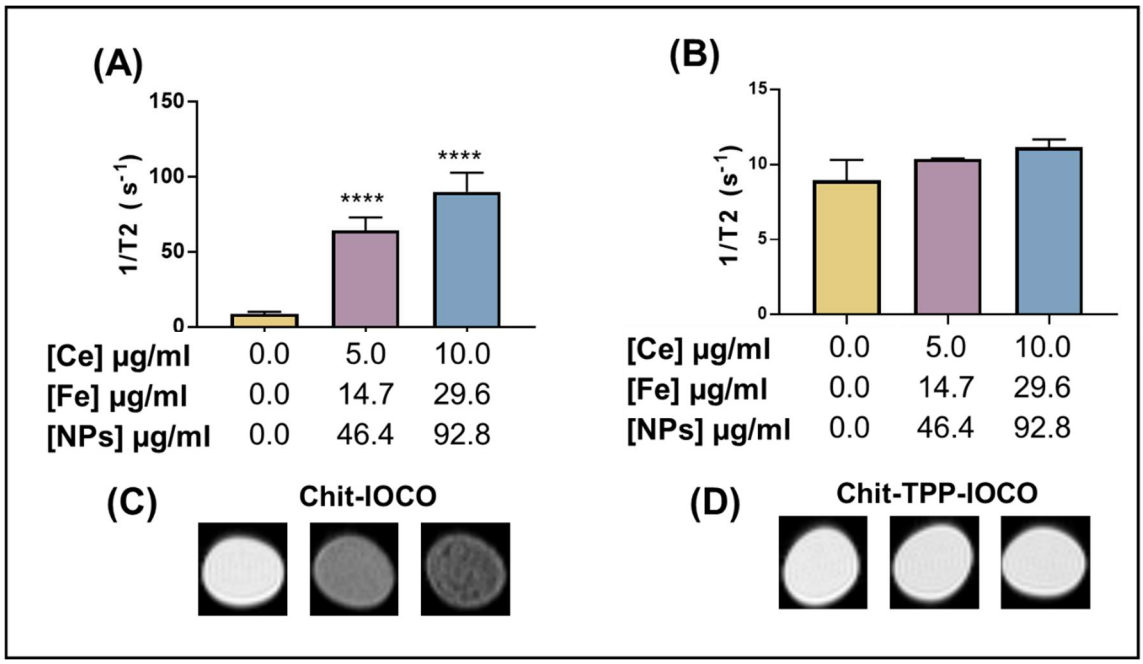

Fig S2. ***In vitro*** **MRI of Chit-IOCO and Chit-TPP-IOCO nanoparticles in RAW264.7 cells. (A)** Graph showing the T_2-weighted MRI signal of RAW264.7 incubated with or without Chit-IOCO in different concentration of Fe. **(B)** Graph showing the T_2-weighted MRI signal of RAW264.7 incubated with or without Chit-TPP-IOCO in different concentration of Fe. **(C)** T_2-weighted MR images of RAW264.7 incubated with Chit-IOCO at different Fe concentrations. **(D)** T_2-weighted MR images of RAW264.7 incubated with Chit-TPP-IOCO at different Fe concentrations. * Compared with [Fe] 0µg/ml: ***$p<0.001$, ****$p<0.0001$

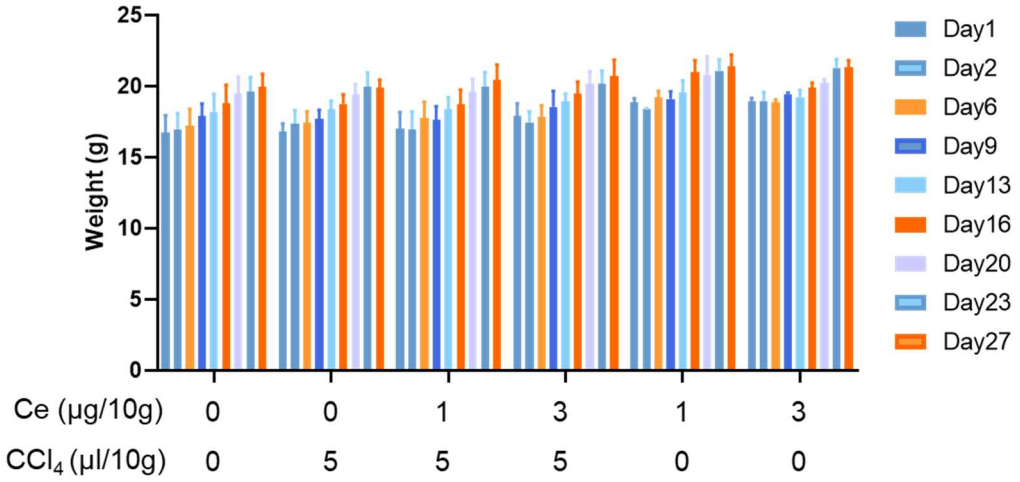

Fig S3. No effect of Chit-IOCO on the weight of C57BL/6 from day 1 to day 27. Mice were treated with different concentrations of Chit-IOCO (cerium concentration: 0 µg/10g, 1 µg/10g and 3 µg/10g). Olive oil injected C57BL/6 mice were used as negative control. Olive oil + CCl_4 injected mice were used as positive control.

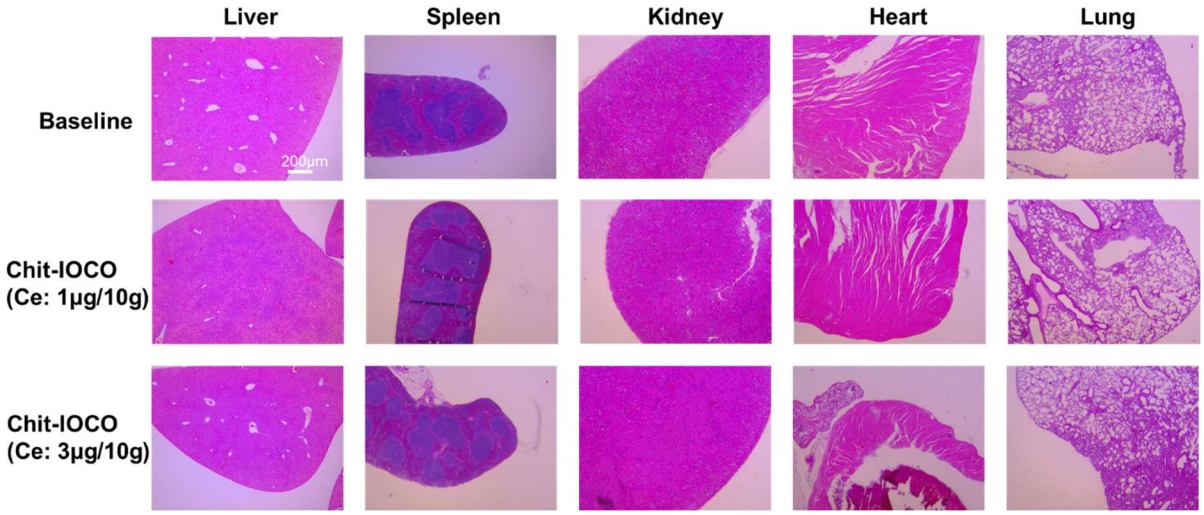

Fig S4. Histopathology (haematoxylin–eosin staining) of organs at 28 days after administration of Chit-IOCO. Mice were treated with or without Chit-IOCO at different concentrations of cerium. At day 28, liver, spleen, kidney, heart and lung of each mice were collected followed by H&E staining. The histopathology photos were then taken by microscopy using a 4x objective.

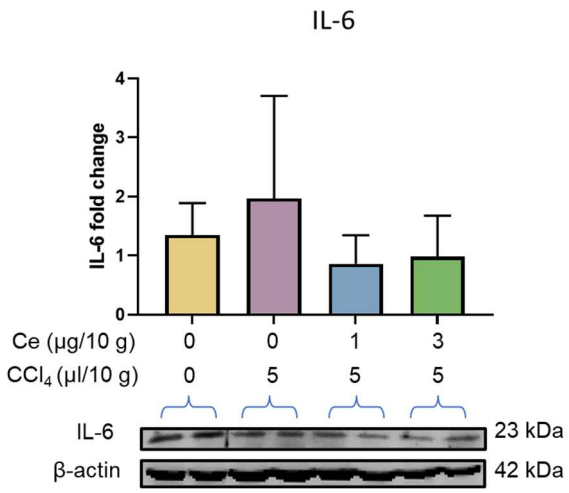

Fig S5. Western blot of IL-6 proteins in CCl_4-induced C57BL/6 mice. The protein expression in the liver of C57BL/6 mice at day 28 was measured via western blot. Graphs showing the IL-6 protein level normalised to β-actin. Images represent western blot for IL-6 and β-actin.

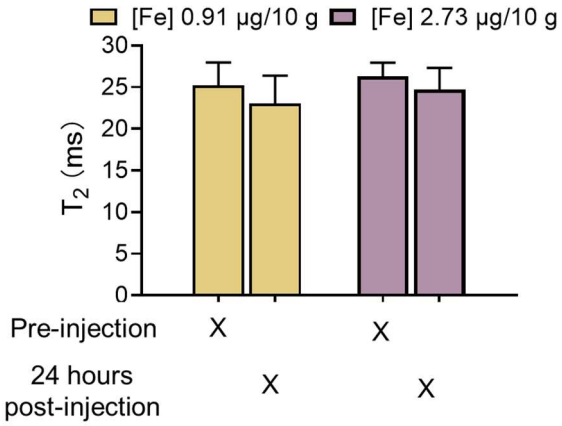

Fig S6. In vivo MRI T_2 contrast ability of Chit-IOCO. Mice were treated with different concentrations of Chit-IOCO (cerium concentration: 1 µg/10g and 3 µg/10g, iron concentration: 0.91 µg/10g and 2.73 µg/10g). MRI T_2 images were acquired before and after injection. Graph showing the T_2 - weighted MRI signal of mice before and one day post injection of Chit-IOCO in different doses.

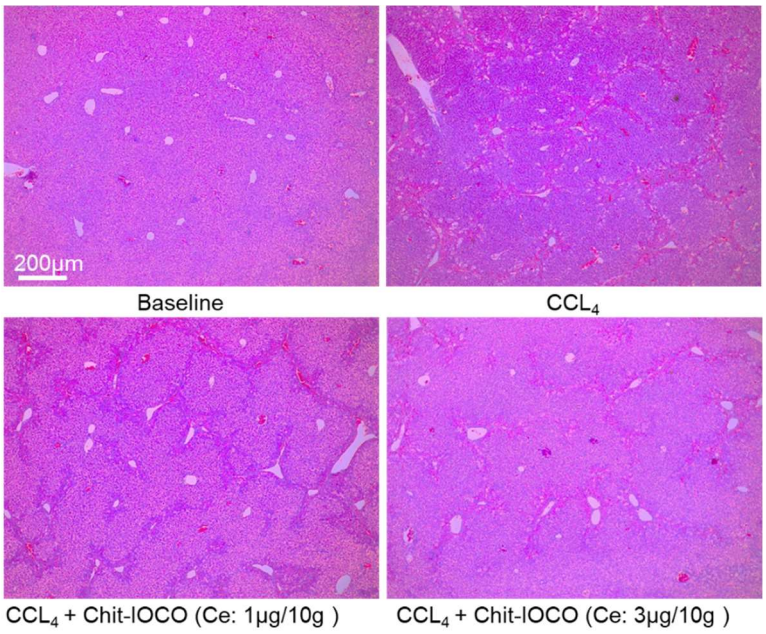

Fig S7. Alleviation of the liver fibrosis at 28 days after administration of different concentrations of Chit-IOCO. Mice were treated with or without CCl_4 and Chit-IOCO at different concentrations of cerium. At day 28, the livers were collected followed by H&E staining. The histopathology photos were then taken by microscopy using a 4x objective.